Available online at www.eccomasproceedia.org
Eccomas Proceedia COMPDYN (2021) 5039-5065

ECCOMAS
Proceedia

COMPDYN 2021
8th ECCOMAS Thematic Conference on
Computational Methods in Structural Dynamics and Earthquake Engineering
M. Papadrakakis, M. Fragiadakis (eds.)
Streamed from Athens, Greece, 28 - 30 June 2021

THREE DIMENSIONAL DYNAMIC INTERACTION OF ADJACENT FOUNDATIONS ON A HALFSPACE WITH LOCAL INHOMOGENEITY APPLYING A COUPLED ITM-FEM APPROACH

Julian Freisinger[1], **Gerhard Müller**[1]

[1] Chair of Structural Mechanics, Technical University of Munich
Arcisstr. 21, 80333 Munich, Germany
e-mail: julian.freisinger@tum.de, gerhard.mueller@tum.de

Abstract. *The dynamic subsoil coupling for a finite number of adjacent foundations has a significant effect on the dynamic behaviour of the foundations involved and the structures based on them. As the mutual influence of the foundations on each other is decisively influenced by the properties and the composition of the subsoil, buried structures or inhomogeneities have to be included, in order to model the real soil conditions as exact as possible and to enable an accurate prediction of the interaction phenomena of adjacent foundations. In this contribution an efficient 2.5D coupled Integral Transform Method (ITM) – Finite Element Method (FEM) approach is used in conjunction with a conventional 3D FEM to compute the dynamic stiffness of foundations resting on the surface of a halfspace including a longitudinally invariant structure or inhomogeneity. Herein, the analytical ITM solutions of the dynamic wave equation allow to account for the infinite extension of the soil by satisfying the radiation condition. The 2.5D FEM formulation enables to model complex, spatially limited structures and a part of the surrounding soil within a cylindrical outer boundary, on which both methods are coupled. The finite foundations on the halfspace surface are modelled using 3D finite elements and are coupled to the soil substructure enforcing the compatibility conditions (full coupling or relaxed boundary conditions) at the common interface. The influence of the embedment depth, size and stiffness of the inclusion on the dynamic response of the foundations, taking into account the through soil coupling, is investigated for different configurations of the surface foundations (distance, width). Frequency dependent compliance functions at the soil-foundation interface are calculated for the different parameter settings and compared with existing solutions to verify the method as well as with the results for the homogeneous halfspace to illustrate the influence of an inclusion. Furthermore the displacement distribution over the total surface of a halfspace with a stiff inclusion due to a dynamic excitation of either one or both of the two considered adjacent rigid surface foundations obtained by a post-processing procedure is presented.*

Keywords: Soil Dynamics, Soil-Structure-Interaction (SSI), Integral-Transform-Method (ITM), Finite-Element-Method (FEM), Foundation-Soil-Foundation Interaction (FSFI), Vibration Mitigation, Wave Impeding Block (WIB)

ISSN:2623-3347
Peer-review under responsibility of the organizing committee of COMPDYN 2021.
doi: 10.7712/120121.8848.19126

1 INTRODUCTION

The dynamic interaction of structures based on a single foundation with the supporting homogeneous or stratified soil has been studied extensively in the past applying a variety of different methods as presented e.g. in [1–8]. However, in the dense urban areas buildings are often not well separated from each other and the dynamic foundation-soil-foundation interaction (FSFI) between the closely spaced structures has a significant effect on the dynamic behaviour of the foundations involved and the structures based on them. This mutual influence is decisively influenced by the properties and the composition of the subsoil.

In the literature, various approaches have been employed to investigate the interaction of foundations located on or embedded in a homogeneous or layered halfspace. Warburton et al. [9] were the first to study the dynamic FSFI of two neighbouring massive foundations resting on a homogeneous halfspace applying an approximate analytical method based on the Bycroft model. The cross interaction of multi-foundation systems located on a viscoelastic stratum due to different excitation types has been investigated by Kobori et al. [10]. Wong and Luco [11] analysed the effect of a layered halfspace on the interaction of two rigid, square surface foundations subjected to external forces by the boundary integral equation technique. Kausel et al. [12] and Lin et al. [13] used the Finite-Element-Method (FEM) together with consistent boundaries to examine the FSFI of rigid foundations resting on or embedded in a stratum over bedrock for harmonic force and moment excitation in all degrees of freedom. An analytical method addressing the dynamic subsoil coupling between a finite number of rigid, rectangular foundations solving the mixed boundary value problem by the Bubnov-Galerkin method has been presented by Triantafyllidis and Prange [14]. The Boundary Element Method (BEM) in the frequency domain has been employed to investigate the 3D FSFI of two adjacent rigid, surface foundations resting on a soil layer over bedrock by Karabalis and Beskos [15] and on a homogeneous halfspace due to seismic resp. harmonic excitation by Qian and Beskos [16] and Qian et al. [17]. Wang et al. [18] also used the BEM to investigate the cross interaction of flexible strip foundations embedded in a homogeneous halfspace. A coupled FEM-BEM approch for the 3D dynamic interaction of two surface foundations in the time domain was presented by Rizos and Wang [19]. More recently Chen et al. [20] employed a time domain Scaled-Boundary-Finite-Element-Method (SBFEM) to investigate the response of two strip foundations embedded in a layered soil. Sbartai [21] coupled the BEM to the Thin-Layer-Method (TLM) to account for the interaction of two embedded, rigid 3D foundations within a layered soil over bedrock. A precise integration method (PIM) is used by Han et al. [22] to analyse the FSFI of a group of adjacent massless and massive 3D foundations on multilayered ground. Radisic [23] uses the Integral-Transform-Method (ITM) together with a kinematic conditions for the deformation of a rigid foundation to investigate the mutual influence of adjacent foundations.

In reality the ground often contains local inhomogeneities and structures, that have an effect on the wave propagation within the soil. Diffraction and scattering lead to an amplification of the initial vibrations and thus significantly influence both, the distribution and the amplitude of the stresses and displacements near the surface and within the surface foundations. Therefore, in order to model the real soil conditions as exact as possible and to enable an accurate prediction of the interaction phenomena of adjacent foundations, these buried structures or inhomogeneities have to be included in the model. The interaction of foundations on a soil including a spatially limited structure has been investigated in literature mainly in the context of Wave Impeding Blocks (WIB). Chouw et al. [24] used the BEM to analyse the vibration transmission in a soil layer over bedrock caused by a harmonic excitation of a rigid strip foundation and found,

that no wave propagation occurs in the layer, if the excitation frequency is lower than the first eigenfrequency (”cutoff frequency”) of the stratum. This effect was used in Chouw and Schmid [25], where a spatially limited WIB was implemented into the soil in order to mitigate the low frequency vibration transmission, induced by the active of two foundations, and thus reduce the dynamic response of the passive foundation. Takemiya and Fujiwara [26] applied a 2D time domain BEM to examine the effect of a single or multiple WIBs located directly beneath or sideways under a rigid strip foundation on a homogeneous halfspace or soil stratum on the response of the system due to an excitation with an impulse load. A 3D BEM frequency domain approach was used by Antes and von Estorff [27] to study the influence of the stiffness of a finite block shaped elastic inclusion within a homogenous halfspace on the dynamic response of a elastic surface foundation. In Peplow and Finnveden [28] a 2D Spectral Finite Element Method (SFEM) is presented analysing the attenuation of surface vibrations by placing a WIB in the near field of the harmonic load applied at the surface of a layered soil stratum. Gao et al. [29] published a 3D BEM, based on Green’s functions deduced with the TLM, which allows it to investigate the dynamic interaction of a surface foundation with a WIB located within a saturated, layered ground as well as to predict the vibration screening effectiveness of the WIB for different parameter settings.

In this study a coupled 2.5D ITM-FEM approach in conjunction with a conventional 3D FEM is presented to examine the influence of a local length invariant structure or inhomogeneity buried in the soil on the dynamic response of three dimensional, finite surface foundations. The 2.5D ITM-FEM approach is used to compute the dynamic stiffness at the discretization points within the interaction areas of the foundations with the soil substructure by evaluating its dynamic response due to concentrated harmonic loads. Therefore all interaction phenomena, including the interaction of the induced waves with the buried structure or inhomogeneity, are comprised. The analytical ITM solutions of the dynamic wave equation allow to account for the infinite extension of the soil by satisfying the radiation condition and thus avoid non-physical reflections at artificial boundaries. A 2.5D FEM formulation enables to model complex, spatially limited structures and a part of the surrounding soil within a cylindrical outer boundary, on which both methods are coupled. The foundations at the soil surface are modelled using common 3D finite elements and are coupled to the soil substructure enforcing the compatibility conditions at the common interface, whereby full coupling or relaxed boundary conditions can be applied.

The outline of the paper is as follows. In subsection 2.1 firstly the fundamental ITM solutions are introduced and superposed in order to obtain the stiffness matrix of a halfspace with cylindrical cavity. Subsequently in 2.2 the dynamic stiffness of the 2.5D FEM subsystem is used to model the embedded inclusion is presented, followed by the coupling of the substructures 2.3. In subsection 3.1 the dynamic stiffness of the soil substructure at the contact areas with the foundations is determined and coupled with the dynamic stiffness of the 3D FEM model of the foundations. A post processing procedure which allows to evaluate the displacement field over the total surface of a soil with inclusion due to a harmonic loading of the foundations is presented in subsection 3.3. The accuracy of the proposed method is demonstrated in subsection 4.1 by comparison with literature results for two benchmark examples. In subsection 4.2 the influence of the embedment depth, size and stiffness of the inclusion on the dynamic response of the foundations, also considering the through soil coupling, is investigated for different configurations of the surface foundations (distance, width). Frequency dependent compliance functions at the soil-foundation interface of a soil with inhomogeneity are presented and compared with the results for the homogeneous halfspace to illustrate the influence of the inclusion.

2 ITM-FEM FORMULATION FOR ELASTODYNAMICS

2.1 ITM Substructure

2.1.1 Fundamental Solutions

The Lamé differential equation describes the dynamic behaviour of a linear elastic, homogeneous and isotropic continuum, which consists of three coupled partial differential equations

$$\mu u^i|^j_j + (\lambda + \mu)\, u^j|^i_j - \rho \ddot{u}^i = 0 \tag{1}$$

with the displacement field u^i, the Lamé constants μ and λ and the density ρ. The differential equations are decoupled using a Helmholtz decomposition $u^i = \Phi|^i + \Psi_l|_k\, \varepsilon^{ikl}$ and thereby expressing the displacement field by the sum of the gradient of a scalar field Φ and the rotation of a vector field $\mathbf{\Psi}$, resulting in an uncoupled system of three wave equations (setting $\Psi_z = 0$ cp. [30]) only depending on the compressional and the shear wave velocities c_p and c_s.

$$\Phi|^j_j - \frac{1}{c_p^2}\ddot{\Phi} = 0 \qquad\qquad \Psi_i|^j_j - \frac{1}{c_s^2}\ddot{\Psi} = 0 \tag{2}$$

The system halfspace is solved in Cartesian coordinates (x, y, z) and is derived from Eq. (2) applying a threefold Fourier transform into the wavenumber-frequency domain (k_x, k_y, z, ω). Thus the coupled partial differential equations turn into three decoupled ordinary differential equations that can be solved analytically with an exponential approach [31]:

$$\hat{\Phi} = A_1\, \mathrm{e}^{\lambda_1 z} + A_2\, \mathrm{e}^{-\lambda_1 z} \qquad\qquad \hat{\Psi}_\alpha = B_{\alpha 1}\, \mathrm{e}^{\lambda_2 z} + B_{\alpha 2}\, \mathrm{e}^{-\lambda_2 z} \tag{3}$$

with $\alpha = x, y$, $\lambda_1 = \left({k_x}^2 + {k_y}^2 - k_p^2\right)^{-2}$, $\lambda_2 = \left({k_x}^2 + {k_y}^2 - k_s^2\right)^{-2}$ and $k_p = \frac{\omega}{c_p}$, $k_s = \frac{\omega}{c_s}$. The wavenumbers are given as $k_x = o\Delta k_x$ with $o = -N_x/2, ..., (N_x/2-1)$ and $k_y = s\Delta k_y$ with $s = -N_y/2, ..., (N_y/2-1)$, where N_x, N_y is the number of Fourier series members or sample points in the original domain respectively. Applying the local boundary conditions on the halfspace surface Λ as well as the Sommerfeld radiation condition [32] the unknown coefficients can be determined and the stresses and displacements within the halfspace can be calculated by $\hat{\boldsymbol{\sigma}}_{\mathbf{hs}} = \hat{\mathbf{K}}_{\mathbf{hs}}\hat{\mathbf{C}}_{\mathbf{hs}}$ and $\hat{\mathbf{u}}_{\mathbf{hs}} = \hat{\mathbf{H}}_{\mathbf{hs}}\hat{\mathbf{C}}_{\mathbf{hs}}$ using the matrices given in [33], where $\hat{\mathbf{K}}_{\mathbf{hs}}$ and $\hat{\mathbf{H}}_{\mathbf{hs}}$ include the fundamental solutions, kinematic and material relations linking the unknowns with the stresses and the displacements. Quantities in the single, twofold resp. threefold Fourier transformed domain are marked with $\bar{}$, $\tilde{}$ and $\hat{}$.

The system fullspace with cylindrical cavity is solved in cylindrical coordinates (x, r, φ) applying a Fourier transform with respect to x and t as well as performing a Fourier series expansion along the cylinder circumference $\varphi \to n$. Furthermore the vector field $\mathbf{\Psi} = \Psi\mathbf{g}^1 + \chi|^j\varepsilon_{ij1}\mathbf{g}^i$ is expressed by two independent scalar fields. The respective system of equations in the (k_x, r, n, ω) domain is solved with Hankel functions of first and second kind [34]:

$$\hat{\Phi}\,(k_x, r, n, \omega) = C_{1n}\, H_n^{(1)}\,(k_1 r) + C_{4n}\, H_n^{(2)}\,(k_1 r) \tag{4}$$

$$\hat{\psi}\,(k_x, r, n, \omega) = C_{2n}\, H_n^{(1)}\,(k_2 r) + C_{5n}\, H_n^{(2)}\,(k_2 r) \tag{5}$$

$$\hat{\chi}\,(k_x, r, n, \omega) = C_{3n}\, H_n^{(1)}\,(k_2 r) + C_{6n}\, H_n^{(2)}\,(k_2 r) \tag{6}$$

with ${k_1}^2 = {k_p}^2 - {k_x}^2$ respectively ${k_2}^2 = {k_s}^2 - {k_x}^2$. Applying the local boundary conditions at the cylinder surface Γ as well as the radiation condition the stresses and displacements can be determined as $\hat{\boldsymbol{\sigma}}_{\mathbf{c}} = \hat{\mathbf{K}}_{\mathbf{c}}\mathbf{C}_{\mathbf{c}}$ and $\hat{\mathbf{u}}_{\mathbf{c}} = \hat{\mathbf{H}}_{\mathbf{c}}\mathbf{C}_{\mathbf{c}}$ as given in [33].
For a more detailed derivation of the fundamental solutions the reader is referred to [33–36].

2.1.2 Superposition of Fundamental Systems

In order to obtain a stiffness matrix for the system halfspace with cylindrical cavity the fundamental solutions presented in 2.1.1 are now superposed in order to satisfy the boundary conditions of the final system on the surface of the halfspace Λ and the cylindrical cavity Γ. For this reason fictitious surfaces $\delta\Lambda$ resp. $\delta\Gamma$ are introduced into the fundamental systems allowing a superposition at the common surfaces as depicted in Figure 1. Thus, unit stress states $\hat{\boldsymbol{\sigma}}_\Lambda$ are

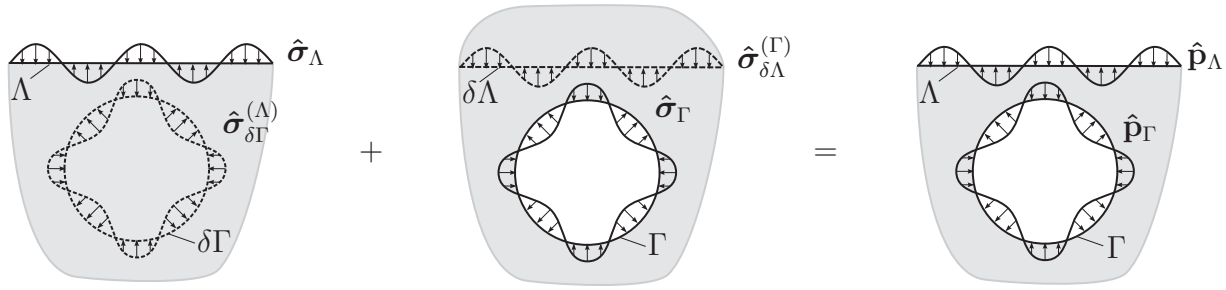

Figure 1: Fictitious surfaces and stresses in the fundamental systems halfspace and fullspace with cylindrical cavity for superposition to a halfspace with cylindrical cavity.

applied at Λ for each wavenumber combination (k_x, k_y) and the stresses $\hat{\boldsymbol{\sigma}}_{\delta\Gamma}^{(\Lambda)}$ at the fictitious surface $\delta\Gamma$ are determined. Reciprocally, the stresses $\hat{\boldsymbol{\sigma}}_{\delta\Lambda}^{(\Gamma)}$ at $\delta\Lambda$ due to unit stress states $\hat{\boldsymbol{\sigma}}_\Gamma$ at Γ for each series member n can be calculated. The sum of the stresses at Λ and Γ has then to coincide with the external loads $\hat{\mathbf{p}}_\Lambda$ and $\hat{\mathbf{p}}_\Gamma$ acting on the total system.

$$\mathbf{C}_\Lambda \hat{\boldsymbol{\sigma}}_\Lambda \quad + \mathbf{C}_\Gamma \hat{\boldsymbol{\sigma}}_{\delta\Lambda}^{(\Gamma)} = \hat{\mathbf{p}}_\Lambda \tag{7}$$

$$\mathbf{C}_\Lambda \hat{\boldsymbol{\sigma}}_{\delta\Gamma}^{(\Lambda)} + \mathbf{C}_\Gamma \hat{\boldsymbol{\sigma}}_\Gamma \quad = \hat{\mathbf{p}}_\Gamma \tag{8}$$

Thereafter it is possible to determine the amplitudes $\mathbf{C}_{\mathbf{ITM}} = (\mathbf{C}_\Lambda \ \mathbf{C}_\Gamma)^T$ of the unit stresses and the stresses at the fictitious boundaries, gathered in $\hat{\mathbf{S}}_{\mathbf{ITM}}$, in dependency of the total external load $\hat{\mathbf{P}}_{\mathbf{ITM}} = (\hat{\mathbf{p}}_\Lambda \ \ \hat{\mathbf{p}}_\Gamma)^T$ on Λ and Γ as:

$$\mathbf{C}_{\mathbf{ITM}} = \hat{\mathbf{S}}_{\mathbf{ITM}}^{-1} \hat{\mathbf{P}}_{\mathbf{ITM}} \tag{9}$$

Hereinafter, the amplitudes $\mathbf{C}_{\mathbf{ITM}}$ are used to scale the displacements due the unit stresses, gathered in $\hat{\mathbf{U}}_{\mathbf{ITM}}$, finally resulting in the displacements $\hat{\mathbf{u}}_{\mathbf{ITM}}$ of the halfspace with cylindrical cavity at Λ and Γ :

$$\hat{\mathbf{u}}_{\mathbf{ITM}} = \hat{\mathbf{U}}_{\mathbf{ITM}} \mathbf{C}_{\mathbf{ITM}} \tag{10}$$

Combining equations (9) and (10) the stiffness matrix $\hat{\mathbf{K}}_{\mathbf{ITM}} = \hat{\mathbf{S}}_{\mathbf{ITM}} \hat{\mathbf{U}}_{\mathbf{ITM}}^{-1}$ of the ITM subsystem for a halfspace with cylindrical cavity is obtained, giving a direct relation between the displacements and the external loads:

$$\underbrace{\begin{bmatrix} \hat{\mathbf{K}}_{\mathbf{\Lambda\Lambda}_{\mathbf{ITM}}} & \hat{\mathbf{K}}_{\mathbf{\Lambda\Gamma}_{\mathbf{ITM}}} \\ \hat{\mathbf{K}}_{\mathbf{\Gamma\Lambda}_{\mathbf{ITM}}} & \hat{\mathbf{K}}_{\mathbf{\Gamma\Gamma}_{\mathbf{ITM}}} \end{bmatrix}}_{\hat{\mathbf{K}}_{\mathbf{ITM}}} \underbrace{\begin{pmatrix} \hat{\mathbf{u}}_{\mathbf{\Lambda}_{\mathbf{ITM}}} \\ \hat{\mathbf{u}}_{\mathbf{\Gamma}_{\mathbf{ITM}}} \end{pmatrix}}_{\hat{\mathbf{u}}_{\mathbf{ITM}}} = \underbrace{\begin{pmatrix} \hat{\mathbf{P}}_{\mathbf{\Lambda}_{\mathbf{ITM}}} \\ \hat{\mathbf{P}}_{\mathbf{\Gamma}_{\mathbf{ITM}}} \end{pmatrix}}_{\hat{\mathbf{P}}_{\mathbf{ITM}}} \tag{11}$$

2.2 2.5D FEM Substructure

In order to couple a finite element structure to the previously introduced ITM subsystem, both substructures need a matching outer boundary. Therefore the dynamic stiffness matrix of a finite element structure with equally distributed nodes on the cylindrical outer boundary, matching with the discretization points of the ITM on Γ, needs to be computed. The dynamic stiffness matrix of the halfspace with cylindrical cavity was computed in the transformed domain for each combination (k_x, ω). The length invariance of the system allows to reduce the originally 3D computations to a series of 2D calculations for each (k_x, ω), where the information of the third dimension is stored in k_x. This 2.5D approach allows to represent the cylindrical cavity in the original domain by a circular cavity in the transformed domain. Thus modified 2D quadrilateral finite elements with linear shape functions and an additional degree of freedom (DOF) in the length direction, adopted to the Fourier transformed domain (k_x, y, z, ω) as presented in [34], can be used to discretize the cross section. The dynamic stiffness of the 2.5D FEM substructure (with the DOFs separated for the outer boundary Γ and the area inside Ω) can finally be computed as:

$$\begin{bmatrix} \tilde{\mathbf{K}}_{\mathbf{\Gamma\Gamma_{FE}}} & \tilde{\mathbf{K}}_{\mathbf{\Gamma\Omega_{FE}}} \\ \tilde{\mathbf{K}}_{\mathbf{\Omega\Gamma_{FE}}} & \tilde{\mathbf{K}}_{\mathbf{\Omega\Omega_{FE}}} \end{bmatrix} \begin{pmatrix} \tilde{\mathbf{u}}_{\mathbf{\Gamma_{FE}}} \\ \tilde{\mathbf{u}}_{\mathbf{\Omega_{FE}}} \end{pmatrix} = \begin{pmatrix} \tilde{\mathbf{P}}_{\mathbf{\Gamma_{FE}}} \\ \tilde{\mathbf{P}}_{\mathbf{\Omega_{FE}}} \end{pmatrix} \tag{12}$$

2.3 Coupling of Substructures

The coupling of the ITM and the FEM substructure is carried out at the two dimensional circular coupling surface Γ in the reference frame of the ITM. Therefore the dynamic stiffness matrix of the FEM subsystem on Γ needs to be transformed into the (k_x, r, n, ω) domain by applying a transformation to a cylindrical reference frame as well as a Fourier series expansion along the circumference. The FEM formulation inside the structure Ω is kept in the (k_x, y, z, ω) domain (Figure 2).

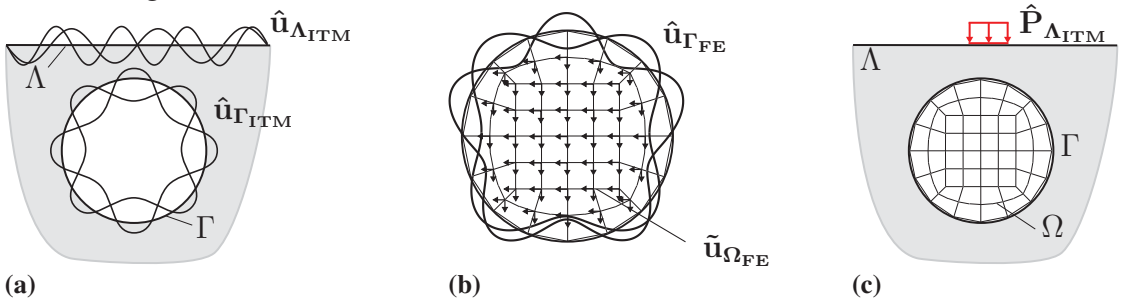

Figure 2: (a) Displacements $\hat{\mathbf{u}}_{\mathbf{\Lambda_{ITM}}}(k_x, k_y, z, \omega)$ on Λ and $\hat{\mathbf{u}}_{\mathbf{\Gamma_{ITM}}}(k_x, r, n, \omega)$ on Γ of the ITM substructure, (b) $\hat{\mathbf{u}}_{\mathbf{\Gamma_{FE}}}(k_x, r, n, \omega)$ on Γ and $\tilde{\mathbf{u}}_{\mathbf{\Omega_{FE}}}(k_x, y, z, \omega)$ within Ω of the FEM substructure in the respective reference systems for the coupling on the circular interaction surface Γ. (c) Halfspace with cylindrical inclusion modelled by the coupled 2.5D ITM-FEM approach.

Thereafter, the continuity of displacements as well as the equilibrium of forces are applied at the coupling surface, finally leading to the total dynamic stiffness matrix of the 2.5D ITM-FEM system of a halfspace with cylindrical cavity filled with finite elements.

$$\underbrace{\begin{bmatrix} \hat{\mathbf{K}}_{\mathbf{\Lambda\Lambda_{ITM}}} & \hat{\mathbf{K}}_{\mathbf{\Lambda\Gamma_{ITM}}} & \mathbf{0} \\ \hat{\mathbf{K}}_{\mathbf{\Gamma\Lambda_{ITM}}} & \hat{\mathbf{K}}_{\mathbf{\Gamma\Gamma_{ITM}}} + \hat{\mathbf{K}}_{\mathbf{\Gamma\Gamma_{FE}}} & \hat{\mathbf{K}}_{\mathbf{\Gamma\Omega_{FE}}} \\ \mathbf{0} & \hat{\mathbf{K}}_{\mathbf{\Omega\Gamma_{FE}}} & \tilde{\mathbf{K}}_{\mathbf{\Omega\Omega_{FE}}} \end{bmatrix}}_{\hat{\mathbf{K}}^{\mathbf{hc}}} \underbrace{\begin{pmatrix} \hat{\mathbf{u}}_{\mathbf{\Lambda_{ITM}}} \\ \hat{\mathbf{u}}_{\mathbf{\Gamma}} \\ \tilde{\mathbf{u}}_{\mathbf{\Omega_{FE}}} \end{pmatrix}}_{\hat{\mathbf{u}}^{\mathbf{hc}}} = \underbrace{\begin{pmatrix} \hat{\mathbf{P}}_{\mathbf{\Lambda_{ITM}}} \\ \hat{\mathbf{P}}_{\mathbf{\Gamma}} \\ \tilde{\mathbf{P}}_{\mathbf{\Omega_{FE}}} \end{pmatrix}}_{\hat{\mathbf{P}}^{\mathbf{hc}}} \tag{13}$$

3 SOIL-FOUNDATION SYSTEM

3.1 Dynamic Soil Flexibility and Stiffness

With the stiffness matrix $\hat{\mathbf{K}}^{\mathbf{hc}}$ it is possible to compute the displacements $\hat{\mathbf{u}}_{\mathbf{\Lambda_{ITM}}}$ on the surface of a halfspace with length invariant FEM inclusion due to an external load $\hat{\mathbf{P}}_{\mathbf{\Lambda_{ITM}}}$ on the ground surface. As the members $\hat{F}^{ij}_{mn}$ with $m, n = x, y, z$ of the complex, dynamic flexibility matrix at the ground surface correspond to the displacements $\hat{u}^i_m$ at a discretization point i on Λ due to a concentrated unit load $\hat{P}^j_n$ in direction n acting at a discretization point j, Eq. (13) can be used in the following to set up the flexibility matrix $\hat{\mathbf{F}}^{ij}_{\mathbf{s}}$ giving the force displacement relationship between a pair of discretization points:

$$\underbrace{\begin{pmatrix} \hat{u}^i_x \\ \hat{u}^i_y \\ \hat{u}^i_z \end{pmatrix}}_{\hat{\mathbf{u}}^i_{\mathbf{s}}} = \underbrace{\begin{pmatrix} \hat{F}^{ij}_{xx} & \hat{F}^{ij}_{xy} & \hat{F}^{ij}_{xz} \\ \hat{F}^{ij}_{yx} & \hat{F}^{ij}_{yy} & \hat{F}^{ij}_{yz} \\ \hat{F}^{ij}_{zx} & \hat{F}^{ij}_{zy} & \hat{F}^{ij}_{zz} \end{pmatrix}}_{\hat{\mathbf{F}}^{ij}_{\mathbf{s}}} \underbrace{\begin{pmatrix} \hat{P}^j_x \\ \hat{P}^j_y \\ \hat{P}^j_z \end{pmatrix}}_{\hat{\mathbf{P}}^j_{\mathbf{s}}} \tag{14}$$

To avoid a singularity under the location of application of the unit load and to keep the numerical errors associated with the discrete calculations small, instead of an unit point force a load uniformly distributed over a small area with a unit resultant is used in the following and referred to as concentrated load [23].

For the later coupling with the finite foundations, modelled by a 3D FEM, the force displacement relationship is needed at the interaction areas of the foundations with the ground surface, as the nodal contact forces and displacements of both substructures must coincide there. Thus, it is necessary, that both substructures exhibit the same discretization at the interaction areas, so that the element nodes of the foundations match with the discretization points of the ITM-FEM soil substructure (Fig. 4), which was discretized on Λ with equidistant points in the original domain (x, y, z, ω). The coordinates of these can be obtained as $x = o\Delta x$ with $o = -N_x/2, ..., (N_x/2 - 1)$ and $y = s\Delta y$ with $s = -N_y/2, ..., (N_y/2 - 1)$, where $\Delta x, \Delta y$ are the incremental distances. Outside of the foundations a traction free surface is assumed.

In order to populate the overall flexibility matrix $\bar{\mathbf{F}}_{\mathbf{s}}$, which fully represents the coupled 2.5D ITM-FEM system and specifies the force-displacement relationship

$$\bar{\mathbf{u}}_{\mathbf{s}}(x, y, \omega) = \bar{\mathbf{F}}_{\mathbf{s}}(x, y, \omega)\, \bar{\mathbf{P}}_{\mathbf{s}}(x, y, \omega) \tag{15}$$

at all $n_{f,\mathrm{tot}} = N_f \cdot n_f$ discretization points within the soil-foundation coupling regions, the soil response $\bar{\mathbf{u}}^i_{\mathbf{s}}$ with $i = 1...n_{f,\mathrm{tot}}$ in all directions at each of these points must be evaluated as a result of a harmonic excitation with concentrated unit loads $\bar{\mathbf{P}}^j_{\mathbf{s}}$ with $j = 1...n_{f,\mathrm{tot}}$ in each spatial direction acting on each of these points in turn. Thereby N_f is the total number of foundations and $n_f = n_{fx} \cdot n_{fy}$ is the number of discretization points of one foundation at the coupling surface with the soil and results from the product of the amount of discretization points of the foundation in x, y-direction n_{fx}, n_{fy}. Since all foundations posses the same size also the number of discretization points is equal. Thus the dimension of $\bar{\mathbf{F}}_{\mathbf{s}}$ yields to $[3n_{f,\mathrm{tot}} \times 3n_{f,\mathrm{tot}}]$.

The displacements and thus also the members of the flexibility matrix, resulting from the application of Eq. (13), are firstly obtained in the (k_x, k_y, z, ω) domain. To enable a direct stiffness coupling by enforcing the compatibility conditions at the interaction areas of the soil with the 3D FEM foundations, it is necessary to have the soil stiffness matrix $\bar{\mathbf{K}}_{\mathbf{s}} = \bar{\mathbf{F}}^{-1}_{\mathbf{s}}$ defined w.r.t. a Cartesian reference frame in the frequency domain (x, y, z, ω) as it is the case for the dynamic stiffness of the foundations. Hence, a twofold inverse Fourier transform (IFFT)

is applied to finally attain the dynamic stiffness matrix $\bar{\mathbf{K}}_{\mathbf{s}}(x, y, z, \omega)$ of the 2.5D ITM-FEM system.

The computational effort to determine the soil flexibility resp. stiffness matrix can be reduced significantly by taking into account the symmetry conditions and in case of the halfspace with inclusion also the length invariance of the system. Instead of placing the concentrated load at each of the $n_{f,\mathrm{tot}}$ discretization points at the contact areas and evaluating the system response at all of them, the foundation areas can be shifted according to the discretization step size, such that every interaction node is positioned once under the unit concentrated load. In case of a homogeneous halfspace, due to the complete rotational symmetry, the position of the load on Λ is irrelevant and the displacement field only needs to be computed twice (once for the load acting in vertical direction and once for one of the horizontal directions, as the other can be determined via the symmetry conditions). In case of the halfspace with inclusion due to the inhomogeneity in the soil, the position of the concentrated load on Λ is no more irrelevant for the resulting displacement field. However, as the system is length invariant only a different position in y-direction causes a different system response. Consequently the concentrated load needs to be placed once at each $y-$discretization point of the foundations. For two foundations located symmetrically w.r.t. the $x-$axis, it is even sufficient to only consider the $y-$ discretization points of one foundation for the load positions, as the results for the second foundation again can be gained by symmetry considerations. Nevertheless, all load directions have to be considered.

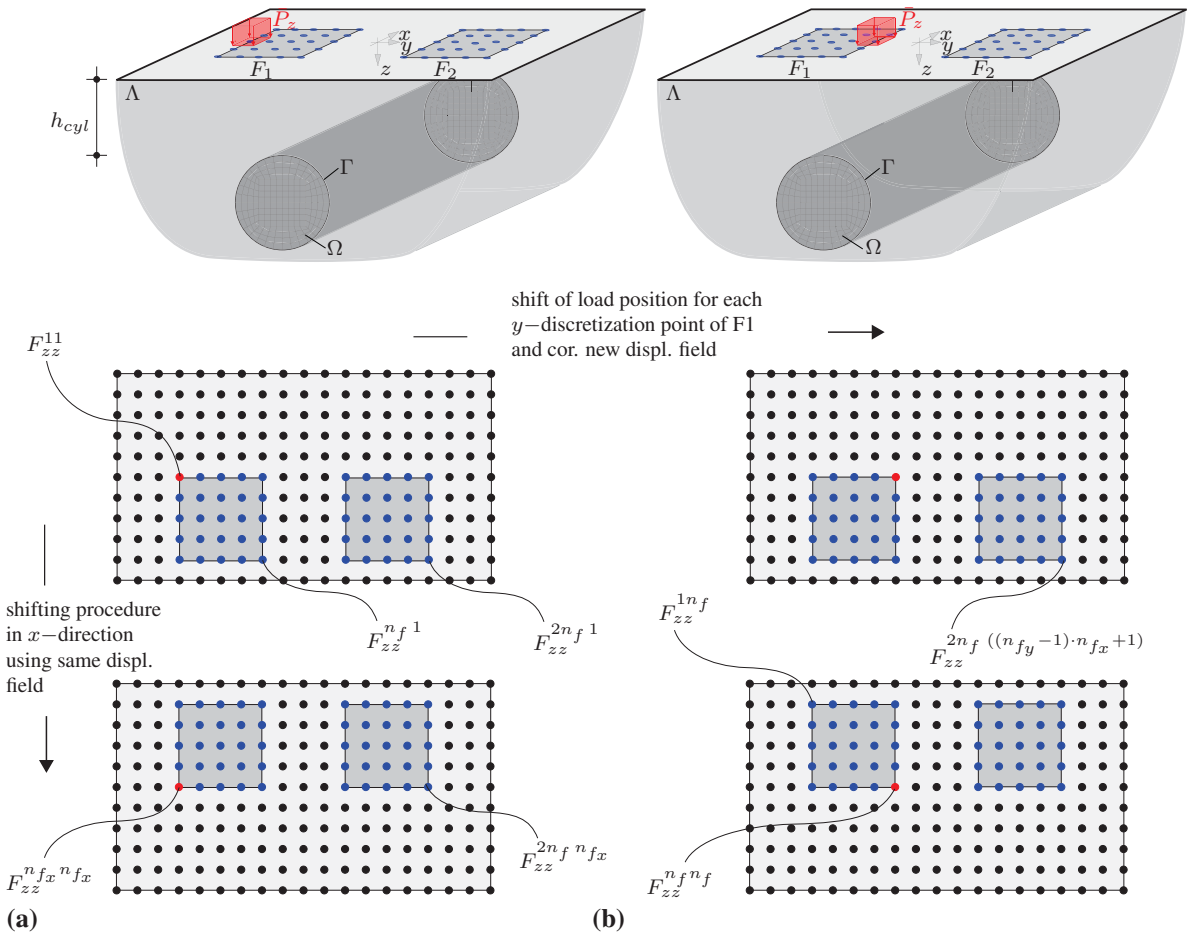

Figure 3: Shifting procedure and selection of displacements for (a) concentrated load at first and (b) last load position on discretization points of soil foundation interface in $y-$direction of foundation F_1.

Figure 3 illustrates the shifting procedure for the latter case. The load is positioned one after another on all $y-$discretization points of the first foundation F_1 and the response at all interaction points of both foundations with the soil surface Λ is evaluated. A new displacement field is determined using Eq. (13) for each of this load positions. For the discretization points of the foundation F_1 in $x-$direction the same system response is used and only the evaluation points are shifted under the point of load application. Thereby the displacements at all nodes of the soil foundation contact area due to a single load position in one direction are sorted into the respective column of $\bar{\mathbf{F}}_\mathbf{s}(x, y, z, \omega)$ after the IFFT. To avoid an ill conditioning of the flexibility matrix, which would result from a shift of the load position by only one discretization point in combination with the distributed uniform load (as then the adjacent columns of $\bar{\mathbf{F}}_\mathbf{s}$ contain very similar values), a coarser mesh is introduced for the shifting procedure as proposed by [23]. The displacements w.r.t. the coarse mesh are computed as the mean value of the displacements w.r.t. the fine mesh within an area $A = n_\Delta \mathrm{d}x \, n_\Delta \mathrm{d}y$. Thereby $\mathrm{d}x, \mathrm{d}y$ are the discretization step sizes of the fine mesh and n_Δ is the factor relating the old step size with the new one.

3.2 Dynamic Stiffness of Soil-Foundation-System

The three dimensional, finite surface foundations, that shall be coupled to the 2.5D ITM-FEM soil substructure, are modelled with conventional finite elements. Either 8-node solid elements or shell elements can be used for this objective. As in this work only foundations satisfying the thin plate assumptions are investigated, a shell element with six DOFs per node presented by Rojas et al. [37] is used due to reasons of computational efficiency. Assembling the element stiffnesses of all elements of one foundation n, the total dynamic stiffness matrix results as

$$\bar{\mathbf{K}}_{\mathbf{f_n}}(\omega) = \mathbf{K}_{\mathbf{f_n}} - \omega^2 \mathbf{M}_{\mathbf{f_n}} \tag{16}$$

with $\mathbf{K}_{\mathbf{f_n}}$ and $\mathbf{M}_{\mathbf{f_n}}$ being the stiffness and the mass matrix of the respective foundation n and ω as the excitation frequency.

The material properties of the foundations are fully described by the linear elastic parameters, i.e. the Young's Modulus E_f, the Poisson ratio ν_f and the density ρ_f. For the following investigations only very stiff (subsequently termed as rigid), massless foundations are considered by assigning them a very high modulus of elasticity and close to zero density. However, it is easily possible with the presented approach, to also include elastic, hysteretically damped foundations with mass into the investigations.

For the coupling of the foundations and the soil substructure, the compatibility conditions need to be satisfied at the interaction nodes on the soil surface $z = 0$ as illustrated in Fig. 4.

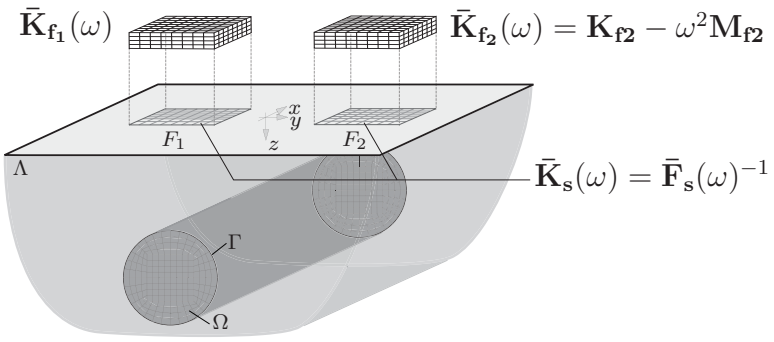

Figure 4: Coupling of FEM foundations F_1 and F_2 to the 2.5D ITM-FEM system of halfspace with stiff cylindrical inclusion at the common interaction surfaces.

Thereby the soil substructure is fully represented by $\bar{\mathbf{K}}_{\mathbf{s}}(x, y, \omega)$, which describes the cross interaction between the foundations under consideration of the interaction via the soil including the inhomogeneity. Since only translational DOFs exist at the discretization points of the soil substructure, the rotational DOFs of the shell elements of the foundations need to be condensed out, before assembling $\bar{\mathbf{K}}_{\mathbf{s}}(\omega)$ and $\bar{\mathbf{K}}_{\mathbf{f_n}}(\omega)$ into the total dynamic stiffness matrix

$$\bar{\mathbf{K}}_{\mathbf{sys}}\, \bar{\mathbf{u}}_{\mathbf{sys}} = \bar{\mathbf{P}}_{\mathbf{sys}} \tag{17}$$

where $\bar{\mathbf{u}}_{\mathbf{sys}}$ is the vector of nodal displacements comprising the DOFs of the foundation nodes and the interface nodes with the soil and $\bar{\mathbf{P}}_{\mathbf{sys}}$ is the respective system load vector. Either full coupling of all DOFs or relaxed boundary conditions (frictionless contact) can be assumed at the interaction surfaces.

3.3 Postprocessing

Firstly the total system of equations in Eq. (17) is solved for the nodal displacements at the soil foundation interfaces $\bar{\mathbf{u}}_{\mathbf{c}} = \bar{\mathbf{u}}_{\mathbf{sys}}(z = 0)$ due to a harmonic load on either one or both foundations. These displacements are used in the following to compute the nodal contact forces $\bar{\mathbf{P}}_{\mathbf{c}} = \bar{\mathbf{K}}_{\mathbf{s}}\, \bar{\mathbf{u}}_{\mathbf{c}}$ w.r.t. the (x, y, z, ω) domain. $\bar{\mathbf{P}}_{\mathbf{c}}$ includes the components in all directions for the full coupling, whereas for relaxed boundary conditions only contact forces in the $z-$direction remain. Subsequently, these nodal contact forces are applied as external loads on the surface of the halfspace with inclusion, as depicted in Fig. 5a, in order to determine the displacements on the whole ground surface Λ by application of Eq. (13). Thereby the effects of the interaction of the foundations with the soil substructure are completely included. However, the members of the stiffness matrix $\hat{\mathbf{K}}^{\mathbf{hc}}$ and the load vector $\hat{\mathbf{P}}^{\mathbf{hc}}$ associated with Λ are given in the Fourier transformed domain. Furthermore, as $\hat{\mathbf{P}}_{\mathbf{\Lambda_{ITM}}}$ in Eq. (13) consists of the stresses on the halfspace surface, the contact forces $\bar{\mathbf{P}}_{\mathbf{c}}$ need to be divided by the corresponding load influence area in a first step and have to be transformed into the (k_x, k_y, z, ω) domain afterwards to obtain the contact stresses $\hat{\boldsymbol{\sigma}}_{\mathbf{c}}(k_x, k_y, z, \omega)$, depicted in Fig. 5b, that can then be sorted into $\hat{\mathbf{P}}_{\mathbf{\Lambda_{ITM}}}$. Therewith the displacements $\hat{\mathbf{u}}_{\mathbf{\Lambda_{ITM}}}(k_x, k_y, z, \omega)$ and finally after a twofold IFFT $\bar{\mathbf{u}}_{\mathbf{\Lambda}}(x, y, z, \omega)$ over the total soil surface Λ can be computed.

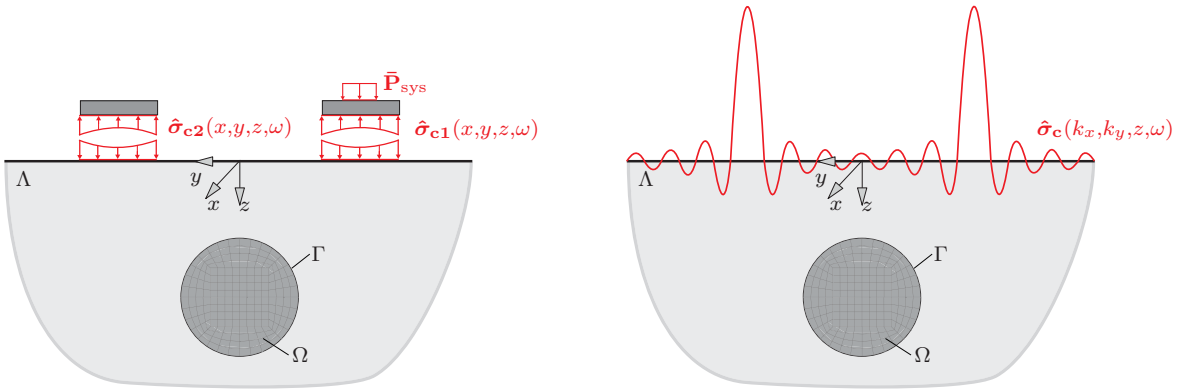

(a) **(b)**

Figure 5: Postprocessing procedure: Application of the contact stresses at the soil foundation interfaces as external load on the 2.5D ITM-FEM system halfspace with inclusion (a) in the original domain (x, y, z, ω) and (b) in the transformed domain $(k_x, k_y, z\omega)$ to determine the displacements $\bar{\mathbf{u}}_{\mathbf{\Lambda}}(x, y, z, \omega)$ over the total ground surface.

4 NUMERICAL RESULTS

In this section the above presented coupled ITM-FEM approach is applied to determine the dynamic response of a single or a group of two adjacent 3D square foundations with a side length B_f, a height h_f and a midpoint distance of d_{f1f2} resting on the surface of a halfspace with a length invariant, cylindrical inclusion of radius R, embedment depth H and a soil covering height h_{cyl}, as depicted in Fig. 6. The material properties of the linear elastic foundations, the soil and the inclusion are described by the Young's modulus E, the Poisson ratio ν and the density ρ. For the soil substructure, whose properties as well as the corresponding wave speeds c_p, c_s and c_r are listed in Tab. 1, additionally material damping was introduced by means of a complex Young's modulus $\hat{E} = E(1 + \mathrm{i}\,\mathrm{sign}(\omega)\zeta)$ with the hysteric damping ratio ζ.

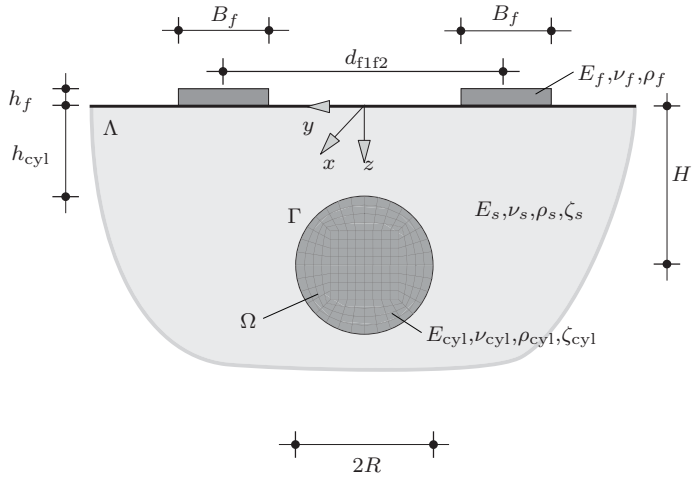

Figure 6: Geometric parameters of the coupled 2.5D ITM-FEM system with two adjacent surface foundations.

For all subsequent calculations, full coupling of all DOFs between soil and foundations is assumed and only rigid, massless square foundations, modelled by choosing a large Young's Modulus E_f, are considered for reason of comparability with other results from literature. However, the limitation to this rather simple systems in this paper does not imply any confinement on the applicability of the proposed method for more complicated SSI and FSFI problems, including flexible and massive structures with rectangular contact area to the soil as well as more complex inclusion geometries inside the 2.5D FEM substructure with cylindrical outer boundary.

	$E\ (\mathrm{N\,m^{-2}})$	$\nu\ ()$	$\rho\ (\mathrm{kg\,m^{-3}})$	$\zeta\ (-)$	$c_p\ (\mathrm{m\,s^{-1}})$	$c_s\ (\mathrm{m\,s^{-1}})$	$c_r\ (\mathrm{m\,s^{-1}})$
Soil	$26.00 \cdot 10^6$	0.30	2000	0.05	132.5	70.8	65.7
Infill A	$96.00 \cdot 10^6$	0.20	2000	0.04	231.0	141.5	128.9
Infill B	$38.40 \cdot 10^7$	0.20	2000	0.04	461.9	282.9	257.9
Infill C	$15.40 \cdot 10^8$	0.20	2000	0.04	925.2	566.5	516.5
Infill D	$34.00 \cdot 10^9$	0.20	2000	0.04	4347.0	2661.9	2426.8
Foundation	$34.00 \cdot 10^{11}$	0.20	1	0.00	$2.142 \cdot 10^6$	$1.145 \cdot 10^6$	-

Table 1: Material parameters of soil, foundation and different inclusion infill materials.

Since only comparably very stiff foundations are considered, all elements of a foundation can be considered as constrained to move like a rigid body and the displacements of each point can be expressed by the displacements and the rotations at the center of the resp. foundation $\bar{\mathbf{u}}^i_{\mathbf{c},\mathbf{r}} = (u^i_x, u^i_y, u^i_z, \varphi^i_x, \varphi^i_y, \varphi^i_z)^T$ at the soil foundation interface $z = 0$. In case of two

adjacent foundations, the displacements $\bar{\mathbf{u}}^i_{\mathbf{c,r}}$ of foundation i due to an external load $\bar{\mathbf{P}}^j_{\mathbf{c,r}} = (P^j_x, P^j_y, P^j_z, M^j_x, M^j_y, M^j_z)^T$ on foundation j with $i, j = 1, 2$ can be computed as

$$\begin{pmatrix} \bar{\mathbf{u}}^{\mathbf{1}}_{\mathbf{c,r}} \\ \bar{\mathbf{u}}^{\mathbf{2}}_{\mathbf{c,r}} \end{pmatrix} = \begin{pmatrix} \bar{\mathbf{F}}^{\mathbf{11}}_{\mathbf{c,r}} & \bar{\mathbf{F}}^{\mathbf{12}}_{\mathbf{c,r}} \\ \bar{\mathbf{F}}^{\mathbf{21}}_{\mathbf{c,r}} & \bar{\mathbf{F}}^{\mathbf{22}}_{\mathbf{c,r}} \end{pmatrix} \begin{pmatrix} \bar{\mathbf{P}}^{\mathbf{1}}_{\mathbf{c,r}} \\ \bar{\mathbf{P}}^{\mathbf{2}}_{\mathbf{c,r}} \end{pmatrix} \tag{18}$$

The main diagonal terms represent the compliance matrices of each rigid foundation itself in case it is loaded with an external load, whereas the off diagonal terms represent the coupling between the foundations. Thereby each member of the total flexibility/compliance matrix of the rigid foundations $\bar{\mathbf{F}}^{ij}_{\mathbf{c,r}}$ consists of

$$\bar{\mathbf{F}}^{ij}_{\mathbf{c,r}} = \begin{pmatrix} \bar{F}^{ij}_{xx} & 0 & 0 & 0 & \bar{F}^{ij}_{x,\varphi_y} & 0 \\ 0 & \bar{F}^{ij}_{yy} & 0 & \bar{F}^{ij}_{y,\varphi_x} & 0 & 0 \\ 0 & 0 & \bar{F}^{ij}_{zz} & 0 & 0 & 0 \\ 0 & \bar{F}^{ij}_{\varphi_x,y} & 0 & \bar{F}^{ij}_{\varphi_x\varphi_x} & 0 & 0 \\ \bar{F}^{ij}_{\varphi_y,x} & 0 & 0 & 0 & \bar{F}^{ij}_{\varphi_y\varphi_y} & 0 \\ 0 & 0 & 0 & 0 & 0 & \bar{F}^{ij}_{\varphi_z\varphi_z} \end{pmatrix} \tag{19}$$

In the entries $\bar{F}^{ij}_{rs}$ the first subscript r indicates the mode of vibration and the second subscript s the direction of the force resp. moment.

For the subsequently presented dimensionless compliance functions, defined as

$$C^{ij}_{rs} = \frac{u^i_r G_s B_f/2}{P^j_s} \tag{20}$$

the displacements u^i_r due to unit force $|P^j_s| = 1$ with $r, s = x, y, z, \varphi_x, \varphi_y, \varphi_z$ normalized with the shear modulus of the soil G_s and the foundation width are evaluated over the dimensionless frequency $a_0 = \omega B_f/c_s$, where c_s is the shear wave velocity of the soil. It is possible to determine the compliance functions for a load either on one or both foundations.

Concerning the dimensions and the discretization of the 2.5D ITM-FEM approach, used to model the soil subsystem, same parameters were chosen for all following computations. A total domain size of $B_x = B_y = 64\ \mathrm{m}$ with $N_x = N_y = 2^9$ discretization points resp. Fourier members was chosen, resulting in a original step size of $\mathrm{d}x = \mathrm{d}y = 0.125\ \mathrm{m}$ at the halfspace surface. With a factor n_Δ, relating the original and the coarse mesh, which is used for the determination of the flexibility, the contact area of each foundation with the soil is meshed with $n_{\mathrm{elem}} = (B_f/(n_\Delta \mathrm{d}x))^2$ quadratic shell elements. The cylindrical 2.5D FEM inclusion was discretized with $N_\varphi = 32$ equidistant nodes resp. Fourier series members along the circumference, leading to an element size between 0.25 and $0.375\ \mathrm{m}$ for the considered inclusion sizes R and thus ca. four elements per shear wave length λ_s of the soil at the highest regarded frequency.

4.1 Validation

In literature numerous results applying a variety of different methods have been published, dealing with the interaction of surface foundations and a homogeneous halfspace. Therefore, the previously presented approach is used in the following to compute the flexibility resp. compliance functions of a single or two adjacent surface foundations resting on a halfspace with inclusion, whereby the material properties of the latter are chosen to be identical to those of the surrounding soil in order to reproduce a homogeneous halfspace. The obtained results are then compared to the literature results to validate the proposed method.

Fig. 7 shows the real and imaginary part of the vertical compliance C_{zz}^{11} of a single rigid, massless square foundation with $B_f = 2$ m on a halfspace with cylindrical inclusion (soil material) with $R = 3$ m and embedment depth $H = 4$ m obtained with the presented 2.5D ITM-FEM approach. A point load with unit amplitude was applied at the midpoint of the foundation for excitation frequencies from 2 to 60 Hz.

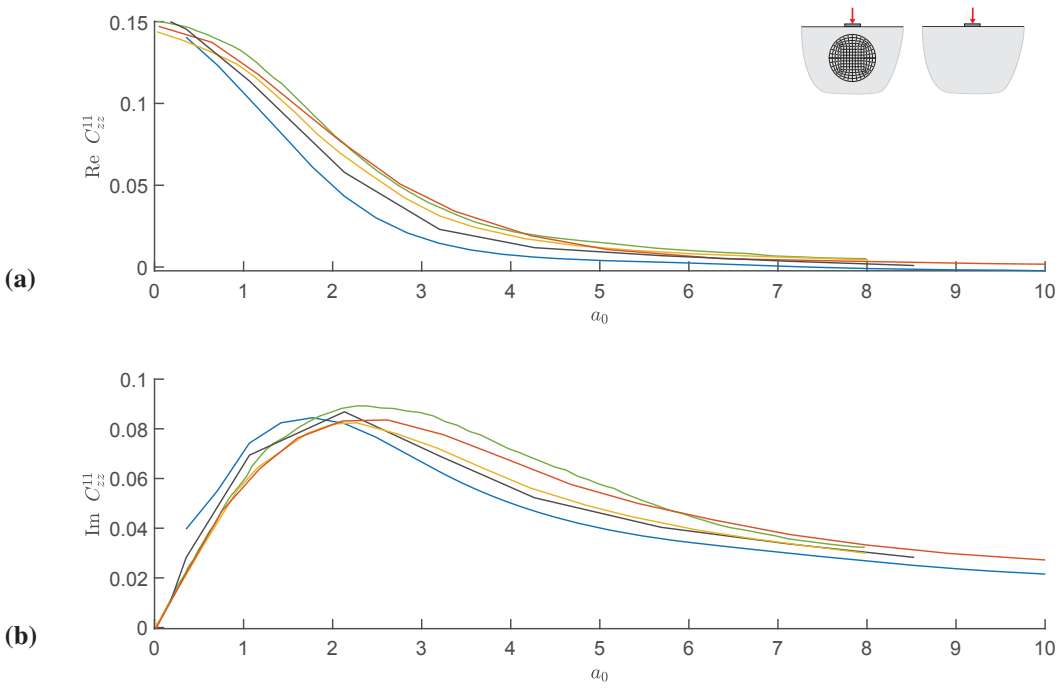

Figure 7: Comparison of real and imaginary part of the vertical compliance functions $C_{zz}^{11}(a_0)$ of a rigid, massless square foundation with $B_f = 2$ m on a halfspace with cylindrical inclusion (Soil) with $R = 3$ m and embedment depth $H = 4$ m obtained with presented ITM-FEM approach with $N_x = N_y = 2^9$ (—) to the results of the ITM-FEM approach on homogeneous halfspace with $N_x = N_y = 2^{11}$ (—), Wong and Luco [1] (—), Hirschauer [38] (—) and Shahi and Noorzad [39] (—).

A good agreement of the results with those obtained by Wong and Luco [1], Hirschauer [38] and Shahi and Noorzad [39] can be observed. However, the compliances attained with the presented method show slightly lower values. One reason for that is the hysteretic material damping ($\zeta = 0.05$), whereas the literature results were determined for zero material damping. In addition, the results for a rigid foundation, determined by enforcing the kinematics of a rigid plate as a displacement boundary condition at the soil-foundation interface of a homogeneous halfspace with lower material damping $\zeta = 0.02$, larger domain size $B_x = B_y = 128$, and larger sample number $N_x = N_y = 2^{11}$ (possible as there the computational effort is much lower) are shown in Fig. 7, whose courses correspond even better with the literature solutions. However, for the halfspace with inclusion due to the rapidly raising computational effort, as the number of $y-$discretization points on the contact surface and thus the load positions, at which a new displacement field for the shifting procedure to populate the flexibility matrix needs to be computed, increases proportional to a decreasing incremental step width, this adaption of the discretization is not reasonable and the agreement of the results gained with the used parameters is considered as sufficient.

In Fig. 8 the absolute value of the vertical compliance of the active (loaded) $|C_{zz}^{11}|$ and the passive (unloaded) $|C_{zz}^{21}|$ of two adjacent surface foundations with distance $d_{\mathrm{f1f2}} = 4$ m due to a unit harmonic point load on foundation F_1 are illustrated. The dimensions of the foundations

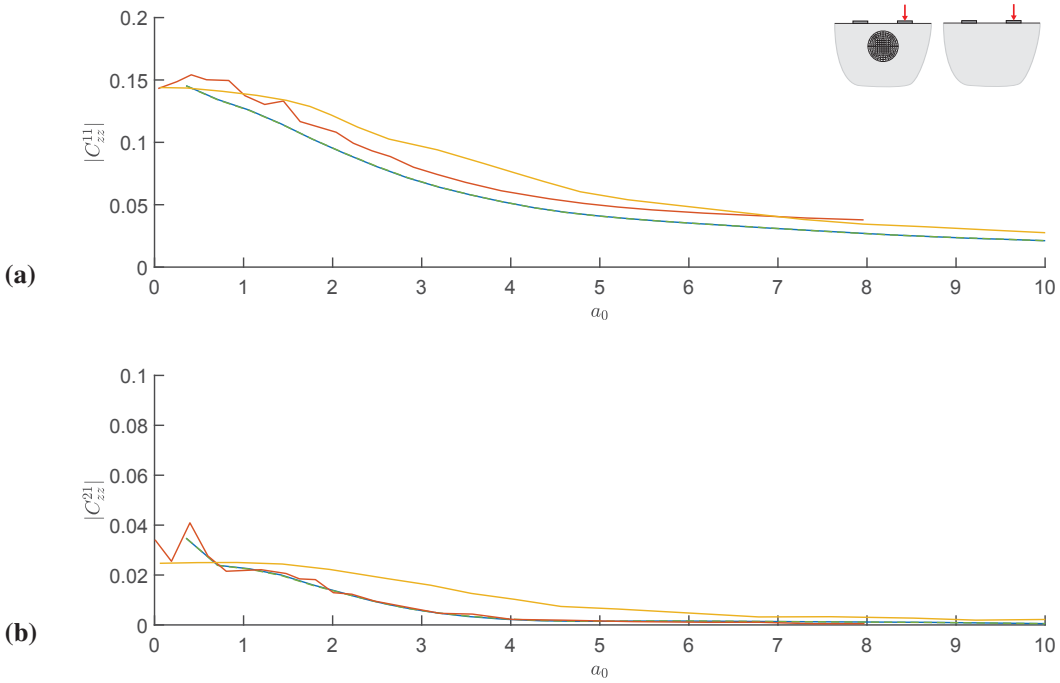

Figure 8: Comparison of absolute vertical compliance functions $|C_{zz}^{ij}(a_0)|$ for (a) first (loaded) and (b) second of two adjacent rigid, massless square foundations with $B_f = 2$ m and distance $d_{\mathrm{f1f2}} = 4$ m on a halfspace with cylindrical inclusion (Soil) with $R = 3$ m and embedment depth $H = 4$ m obtained with presented 2.5D ITM-FEM approach (—) to the results of the ITM approach on homogeneous halfspace, enforcing the kinematic of a rigid plate as displacement boundary condition (– –), Radisic [23] (—) and Karabalis and Mohammadi [40] (—).

as well as the parameters of the halfspace with inclusion are chosen as before. A perfect match of the presented 2.5D ITM-FEM approach with the ITM approach with the kinematic condition can be observed, if same discretization parameters are chosen. Furthermore, the results show good agreement with those obtained by Radisic [23] and Karabalis and Mohammadi [40], who again obtained slightly larger compliances due to zero material damping. At higher frequencies, where mainly the geometrical damping dominates the system response, the deviations diminish.

Overall the comparison with literature results shows, that the proposed method delivers valid results and can further be applied to determine compliance functions of foundations resting on soils with embedded structures or inhomogeneities.

4.2 Parameter study

In this subsection the influence of the variation of the inclusion parameters such as embedment depth H, size R and stiffness E_{cyl} on the dynamic response of a single or two adjacent rigid, massless, square surface foundations, including their cross interaction, is investigated for different configurations of the surface foundations w.r.t. their midpoint distance d_{f1f2} and width B_f. The frequency dependent dimensionless compliance functions at the soil-foundation interface are presented for the different system designs and compared with the results for equivalent foundations resting on a homogeneous halfspace to illustrate the influence of the inclusion respectively the change in influence for varying configurations of inclusion and foundations. Furthermore the impact of a stiff, length invariant cylindrical confinement on the displacement distribution over the entire ground surface as a result of a simultaneous harmonic excitation of both foundations, determined by the post-processing method described above, is presented.

Variation of embedment depth H - single foundation

Firstly the influence of a variation of the embedment depth H of a stiff cylindrical inclusion (Infill D in Tab. 1) directly located beneath a single foundation on the compliance functions is investigated. All other parameters, such as the foundation width $B_f = 2$ m, the inclusion radius $R = 3$ m, as well as the soil and inclusion material are kept constant.

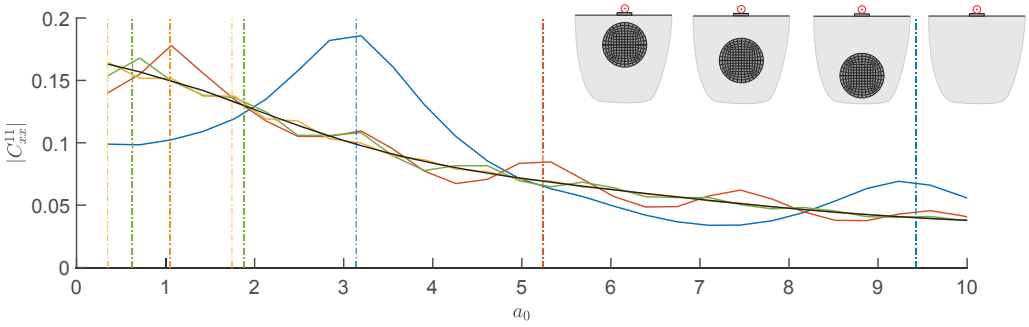

Figure 9: Absolute horizontal compliance functions $|C^{11}_{xx}(a_0)|$ of a rigid, massless square foundation with $B_f = 2$ m on a halfspace with cylindrical inclusion (Infill D) with $R = 3$ m and varying embedment depth $H = 4$ m (—), $H = 6$ m (—), $H = 8$ m (—), $H = 12$ m (—) and on a homogeneous halfspace (—).

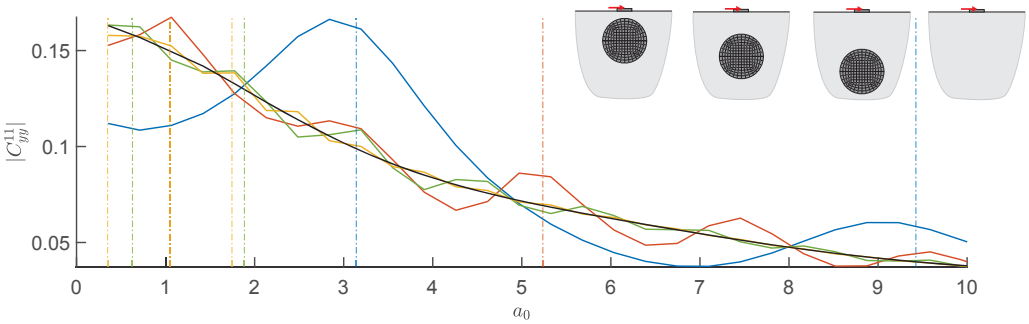

Figure 10: Absolute horizontal compliance functions $|C^{11}_{yy}(a_0)|$ of a rigid, massless square foundation with $B_f = 2$ m on a halfspace with cylindrical inclusion (Infill D) with $R = 3$ m and varying embedment depth $H = 4$ m (—), $H = 6$ m (—), $H = 8$ m (—), $H = 12$ m (—) and on a homogeneous halfspace (—).

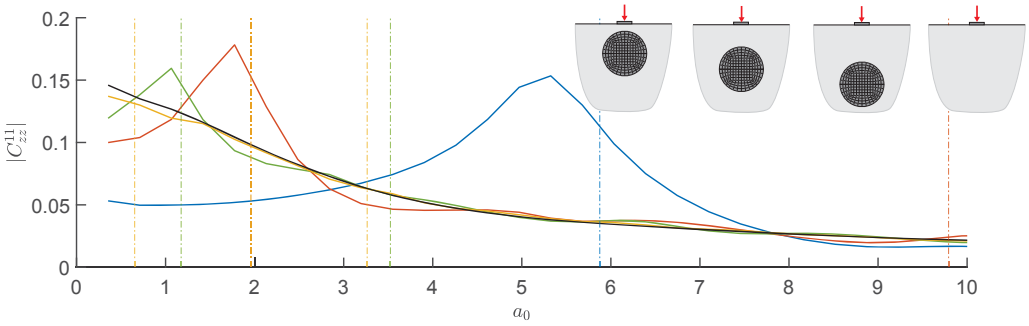

Figure 11: Absolute vertical compliance functions $|C^{11}_{zz}(a_0)|$ of a rigid, massless square foundation with $B_f = 2$ m on a halfspace with cylindrical inclusion (Infill D) with $R = 3$ m and varying embedment depth $H = 4$ m (—), $H = 6$ m (—), $H = 8$ m (—), $H = 12$ m (—) and on a homogeneous halfspace (—).

Figs. 9 and 10 show the horizontal compliance functions due to a harmonic excitation with horizontal unit forces. In case of small embedment depths H, corresponding to a small thicknesses of the soil layer between the stiff inclusion and the bottom of the foundation h_{cyl}, large fluctuations of the flexibilities $|C_{xx}^{11}|$ and $|C_{yy}^{11}|$ can be observed. This large influence of the buried structure on the foundation flexibilities decreases with increasing H, for which the results converge to those obtained for a homogeneous halfspace. However, some waviness in the flexibilities is left, which can be attributed to waves reflected at the soil-inclusion interface and their superposition with the primary waves. The two rather distinct peaks for $H = 4$ can be linked to the first and second horizontal eigenfrequencies of a soil layer over bedrock (defined equal to the natural frequencies of an equivalent one-dimensional rod featuring the same length as the thickness of the layer like proposed in [24] and also depicted in Figs. 9 and 10)

$$f_{\mathrm{h,res}} = \frac{(2n-1)c_s}{4\,H_{\mathrm{layer}}} \quad \text{with} \quad n = 1, 2, ... \tag{21}$$

which here result with $H_{\mathrm{layer}} = h_{\mathrm{cyl}} = 1$ to $f_{\mathrm{h,res}} = 17.7,\ 53.1$ Hz resp. $a_{0,\mathrm{h,res}} = 3.14,\ 9.42$. The generally quite resembling qualitative course of $|C_{xx}^{11}|$ and $|C_{yy}^{11}|$ can be explained by the rather small foundation width $B_f = 2\ \mathrm{m}$ compared to the diameter of the inclusion with $6\ \mathrm{m}$, which leads to a similar behaviour in the $y-$ as in the $x-$direction of the fully length invariant inclusion. Nevertheless, the maxima of $|C_{xx}^{11}|$ are slightly more peaked, show little higher amplitudes and fit better to the horizontal resonance frequencies of a soil layer in Eq. (21).

Also in the vertical compliances $|C_{zz}^{11}|$ in Fig. 11 the existence of vertical resonances of the soil layer over the inclusion is clearly visible. Depending on the embedment depth H, distinct peaks occur in the vicinity of the vertical resonance frequencies of an elastic stratum also depicted in Fig. 11 by the vertical lines

$$f_{\mathrm{v,res}} = \frac{(2n-1)c_p}{4\,H_{\mathrm{layer}}} \quad \text{with} \quad n = 1, 2, ... \tag{22}$$

However, since the cylindrical inclusion is spatially limited in the $y-z-$plane, the behaviour only approximates that of a soil layer over bedrock. This also holds for the corresponding resonance frequencies and explains the shift of the smoother peaks towards lower frequencies. It was shown by Chouw et al. [24] and Kobori et al. [41], that in a perfectly elastic stratum with zero material damping, energy attenuation is only possible by free waves, i.e. Rayleigh and Love waves, travelling in radial direction away from the source and that for an excitation at the surface of the layer with a frequency below the first resonance frequency (”cutoff frequency”) no such propagating waves can occur. The imaginary part of the flexibility at the soil foundation interface, associated with the system damping, in this case directly shows the amount of radiation damping due to propagating waves into the laterally infinite medium and is zero below the first natural frequency. In contrast, in a viscoelastic stratum with non zero material damping even in the low frequency range, below the first natural frequency, innumerable modes of the free propagating waves are possible. Consequently both attenuation mechanisms, material and radiation damping, are present in the whole frequency range. However, in the low frequency range each of these modes is highly damped, such that the dissipative attenuation predominates the radiative one greatly and the energy attenuation due to wave radiation is extremely small [41]. At resonance a significant amplification of the flexibility amplitudes can be observed, which decrease again and converge to the solution for the homogeneous halfspace with increasing frequency. This is because for larger layer thicknesses resp. higher excitation frequencies,

implying a larger ratio of H/λ_p, the waves introduced at the source at the ground surface almost attenuate before reaching the layer boundary resp. the stiff inclusion and only scarcely affect the dynamic response of the system. In this case approximately the same amount of energy is dissipated and dispersed as in case of the homogeneous halfspace. Also for the stiff cylindrical inclusion considered before, an imaginary part of the compliance C_{zz}^{11} in Fig. 12 close to zero can be observed for excitation frequencies below the first vertical resonance frequency. This small values of the imaginary part, which are linked to both, material and geometrical damping, can, according to the above explanations, be associated with an only small dissipative energy attenuation due to material damping in the low frequency range. At resonance, large values of the imaginary part are observed connected to a large amount of dissipated energy, which then is dominated by the energy dispersion of the freely propagating waves occurring from then on. For excitation frequencies, which are large in comparison to the first layer resonance, associated with the respective soil layer thickness h_{cyl}, the compliances converge to the halfspace solution.

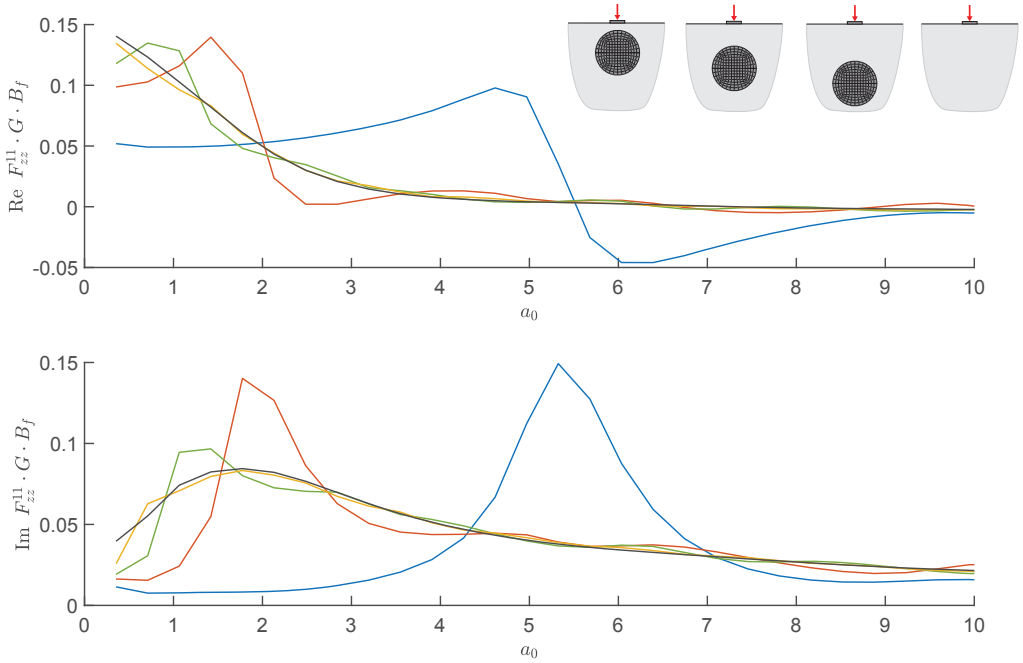

Figure 12: Real and imaginary part of vertical compliance functions $C_{zz}^{11}(a_0)$ of a rigid, massless square foundation with $B_f = 2$ m on a halfspace with cylindrical inclusion (Infill D) with $R = 3$ m and varying embedment depth $H = 4$ m (—), $H = 6$ m (—), $H = 8$ m (—), $H = 12$ m (—) and on a homogeneous halfspace (—).

Variation of embedment depth H - two adjacent foundations

Now the compliance functions of two adjacent surface foundations with a width of $B_f = 2$ m and a midpoint distance $d_{\text{f1f2}} = 8$ m, again resting on a halfspace with a stiff cylindrical inclusion (Infill D) of radius $R = 3$ m and varying embedment depth H are considered.

For the horizontal compliance $|C_{xx}^{11}|$ of the loaded foundation in Fig. 13a, only relatively small deviations from those obtained for the homogeneous halfspace are visible in comparison to the case of the single foundation. This is because here the loaded foundation is located besides the stiff inclusion instead of directly over it. The largest deviations are observed for the smallest embedment depths and in the low frequency range. The then occurring amplification can be traced back to the effect of waves reflected at the inclusion. With increasing H and

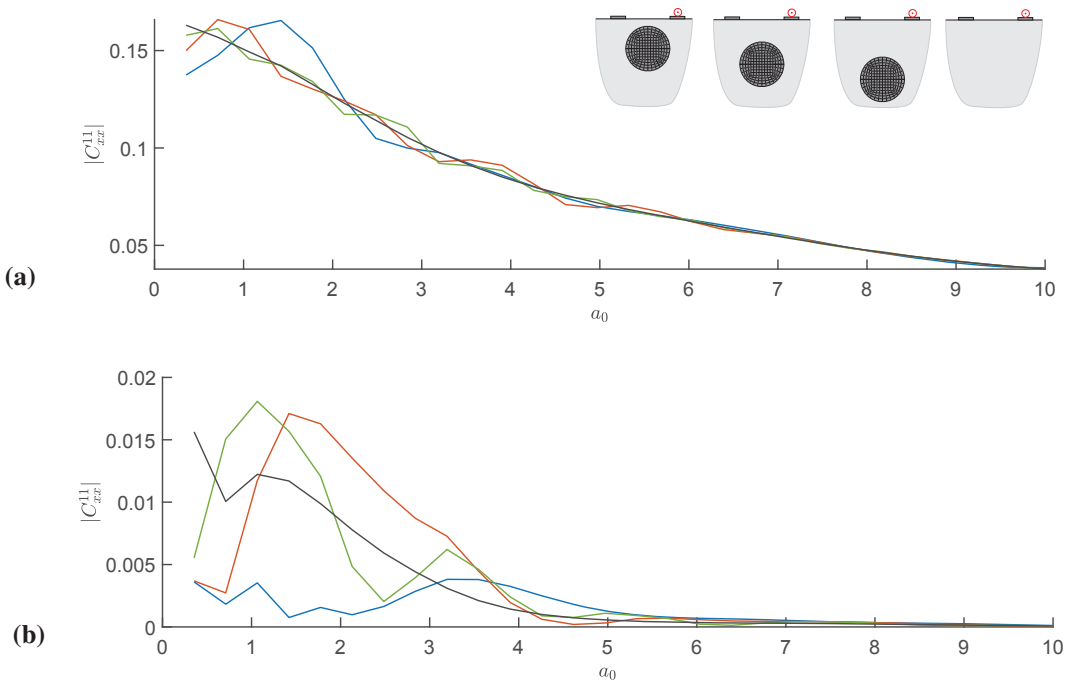

Figure 13: Absolute vertical compliance functions $|C_{xx}^{ij}(a_0)|$ for (a) first (loaded) and (b) second of two adjacent rigid, massless square foundations with $B_f = 2$ m and distance $d_{\mathrm{f1f2}} = 8$ m on halfspace with cylindrical inclusion (Infill D) with $R = 3$ m for varying embedment depth $H = 4$ m (—), $H = 6$ m (—), $H = 8$ m (—) and on a homogeneous halfspace (—).

increasing frequency $|C_{xx}^{11}|$ converges to that for the homogeneous halfspace. The compliance of the passive foundation $|C_{xx}^{21}|$ is very small for small H, as the main excitation takes place in the direction of the length invariant inclusion and a propagation of the elastic waves from the excited foundation F_1 to the unloaded foundation F_2 is disturbed by the cylindrical inclusion in the transmission path. Furthermore in the soil layer over the inclusion propagating waves can occur only above the first (here horizontal) layer resonance frequency, which can e.g. be observed by the increase of $|C_{xx}^{21}|$ for $H = 4$ at excitation frequencies $a_0 > 3.14$. With increasing H the amplitude of $|C_{xx}^{21}|$ in the low frequency range increases due to a smaller shielding effect of the cylindrical inclusion. For intermediate values of H, $|C_{xx}^{21}|$ shows to be larger than in case of a homogeneous halfspace, probably due to reflected waves at the top of the inclusion, amplifying the response at F_2. In case of large H and with increasing frequencies, the compliance again converges to that obtained for the homogeneous halfspace, as with increasing ratio of the soil layer thickness to the elastic wave lengths the influence of the inclusion diminishes.

Comparing the results of for the compliances in $x-$ and $y-$direction, it can be stated, that $|C_{yy}^{11}|$ in Fig. 14 converges to the halfspace solution only at higher frequencies as $|C_{xx}^{11}|$ and the deviations are larger, which is because the direction of excitation in this case directly points towards the inclusion located in the transmission path and thus a bigger portion of elastic waves is reflected as for the excitation in $x-$direction, especially as the foundation is located besides the inclusion. For very low frequencies the inclusion size is small compared to the wavelength, wherefore it has no big influence on the direct cross interaction of the adjacent foundations resulting in higher values of $|C_{yy}^{21}|$. Again a raise of amplitudes for $a_0 > 3.14$ can be observed for $|C_{yy}^{21}|$.

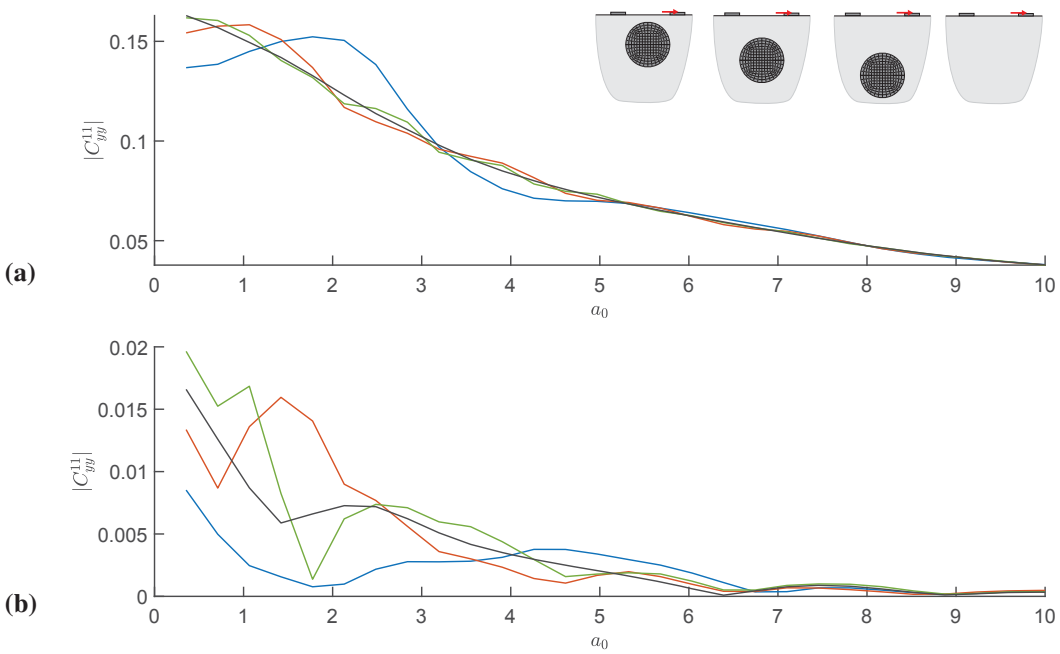

Figure 14: Absolute vertical compliance functions $|C^{ij}_{yy}(a_0)|$ for (a) first (loaded) and (b) second of two adjacent rigid, massless square foundations with $B_f = 2$ m and distance $d_{\mathrm{f1f2}} = 8$ m on halfspace with cylindrical inclusion (Infill D) with $R = 3$ m for varying embedment depth $H = 4$ m (—), $H = 6$ m (—), $H = 8$ m (—) and on a homogeneous halfspace (—).

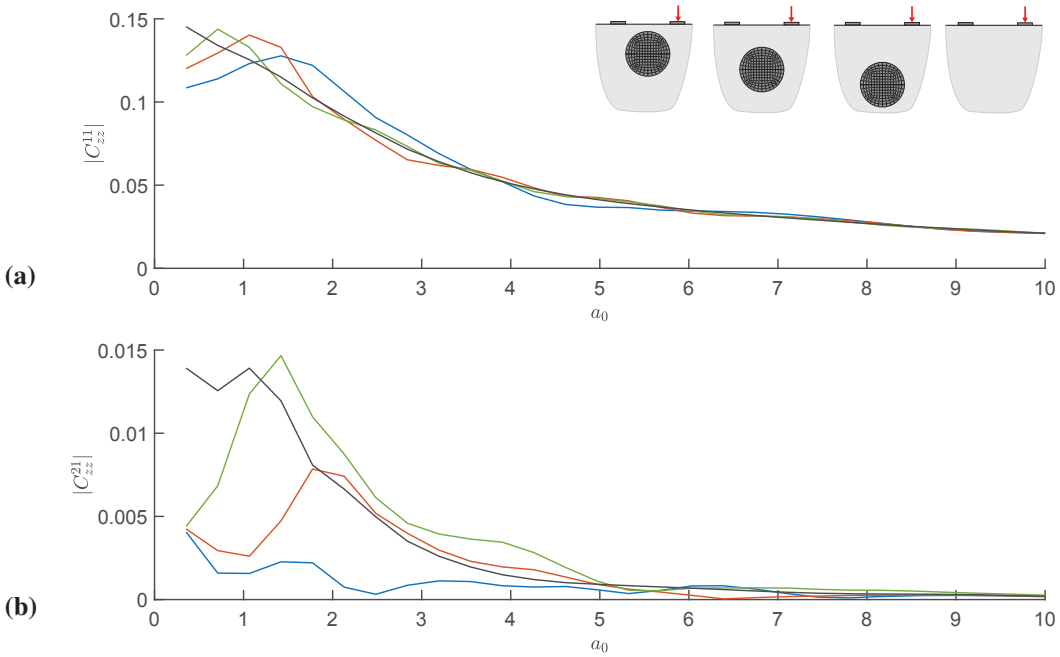

Figure 15: Absolute vertical compliance functions $|C^{ij}_{zz}(a_0)|$ for (a) first (loaded) and (b) second of two adjacent rigid, massless square foundations with $B_f = 2$ m and distance $d_{\mathrm{f1f2}} = 8$ m on halfspace with cylindrical inclusion (Infill D) with $R = 3$ m for varying embedment depth $H = 4$ m (—), $H = 6$ m (—), $H = 8$ m (—) and on a homogeneous halfspace (—).

Concerning the vertical compliances $|C_{zz}^{11}|$ of the active foundation in Fig. 15 only small deviations occur as the foundation is located besides the inclusion and only a little part of the induced elastic waves interacts with it. In general small compliances $|C_{zz}^{21}|$ are observed over the whole frequency range for small H. However, above the first vertical resonance frequency of the soil layer over the inclusion at $a_0 = 5.87$ for $H = 4$ a slight increase of $|C_{zz}^{21}|$ can be observed. The overall trend of the compliances tending to those obtained for the homogeneous halfspace for increasing H and a_0 is also found here.

Due to space limitation for all following cases only the vertical compliances are shown. However the computation of the compliances for any load direction and type is possible.

Variation of the inclusion radius R

Hereinafter, the embedment depth $H = 4$ m of the inclusion under two adjacent surface foundations with $B_f = 2$ m and $d_{\mathrm{f1f2}} = 8$ m is fixed as well as the material properties and only its size R is varied. Fig. 16 shows, that the vertical compliances $|C_{zz}^{11}|$ of the loaded foundation on the soil with the inclusion are very close to those for the homogeneous halfspace for small inclusion size R. Also for the largest considered radius $R = 3$ m, only small deviations occur, as the foundation is located besides the inclusion and the share of waves travelling downwards or to the inclusion averted side (thus not affected by it) is quite large. The compliances $|C_{zz}^{21}|$ of the passive foundation show low amplitudes for large R and converge, due to the effects already pointed out earlier, to those for the homogeneous halfspace with decreasing inclusion size.

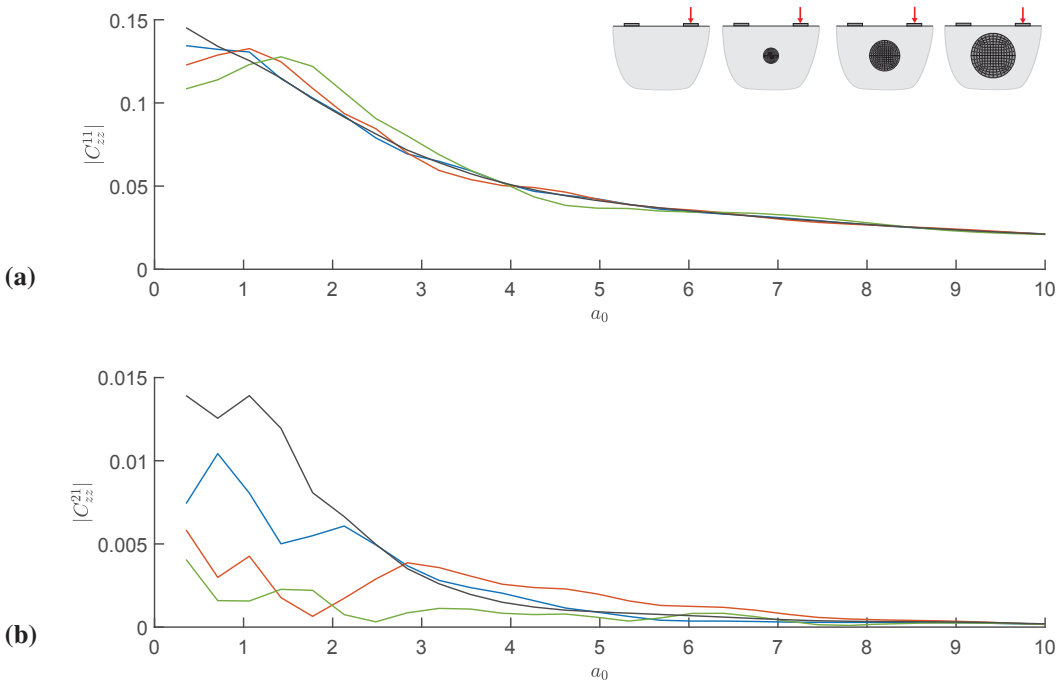

Figure 16: Absolute vertical compliance functions $|C_{zz}^{ij}(a_0)|$ for (a) first (loaded) and (b) second of two adjacent rigid, massless square foundations with $B_f = 2$ m and distance $d_{\mathrm{f1f2}} = 8$ m on halfspace with cylindrical inclusion (Infill D) with embedment depth $H = 4$ m for varying radius $R = 1$ m (—), $R = 2$ m (—), $R = 3$ m (—) and on a homogeneous halfspace (—).

For the system configuration with the maximum inclusion size of $R = 3$, the displacements on the whole ground surface have been determined with the post processing procedure outlined in subsection 3.3 applying relaxed boundary conditions, i.e. frictionless contact at the soil foundation interfaces. The left column of Fig. 17 shows the results for the real part of the vertical displacements, obtained for a harmonic excitation with $f = 6$ Hz of both resp. only one foundation, resting on a homogeneous halfspace. In Fig 17a, a wave propagation concentrated on the direction of the foundation alignment and perpendicular to it can be observed, whereas Fig 17c shows a nearly omnidirectional propagation of the surface waves. The second, unloaded foundation only hardly influences the displacement field on the ground surface, except the area directly under it, where a linear displacement course arises due to the rigidity of the foundation plate. In case of a massive foundation the inertia effects would lead to a much higher influence of the unloaded foundation on the system response. The right column of Fig. 17 shows the results for same foundation and load configuration, but on a halfspace with stiff inclusion. Fig. 17b shows a significant reduction of $u_z(x, y, z = 0, \omega)$ in a limited area along the entire length of the stiff inclusion compared to the case of the homogeneous halfspace, in turn leading to an increase in amplitudes in the direction perpendicular to the inclusion on both sides. Furthermore, the behaviour of the stiff inclusion as wave barrier can clearly be observed in Fig. 17d, where a considerable reduction of $u_z(x, y, z = 0, \omega)$ occurs on the load averted side of the inclusion. These effects gets even more obvious, when the displacements along the $y-$direction for $x = 0$ are compared for both cases in Fig. 18.

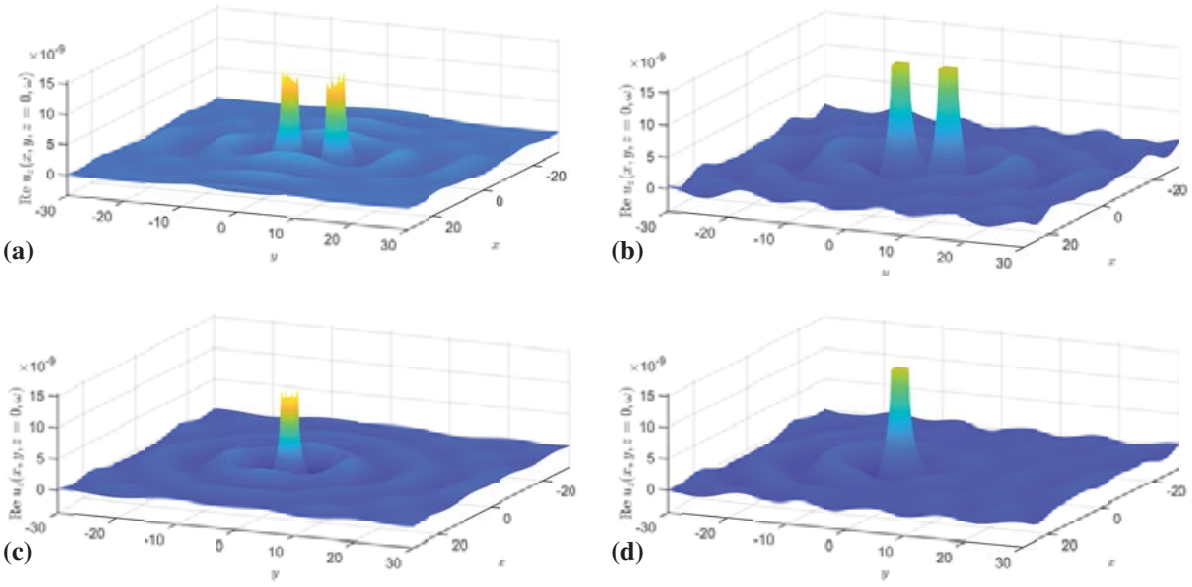

Figure 17: Real part of vertical displacement $u_z(x, y, z = 0, \omega)$ on whole ground surface due to harmonic loading ($f = 6$ Hz) on (a),(b) both and (c),(d) only one of the adjacent rigid, massless foundations with $B_f = 2$ m and $d_{\mathrm{f1f2}} = 8$ m resting on the surface of a (a),(c) homogeneous halfspace and (b),(d) halfspace with a stiff cylindrical inclusion (Infill D) with $H = 4$ m and $R = 3$ m, obtained with the post processing procedure.

Variation of foundation size B_f

Now the width of the foundations is varied, while keeping the midpoint distance $d_{\mathrm{f1f2}} = 8$ m as well as all other parameters constant. Only relatively minor deviations of $|C_{zz}^{11}|$ from the homogeneous halfspace response for $B_f = 2$ and 4 m are observed in Fig. 19. This is

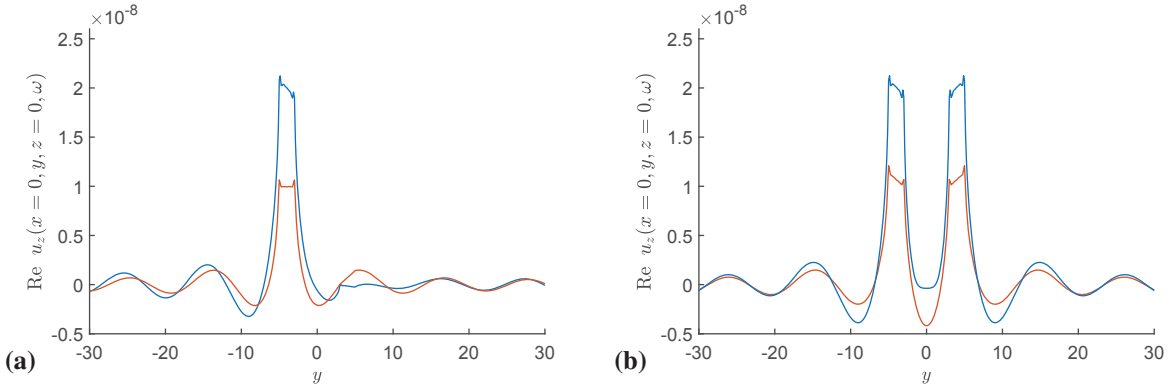

Figure 18: Real part of vertical displacement $u_z(x=0,y,z=0,\omega)$ along $y-$direction for $x=0$ due to harmonic loading with $f=6$ Hz on (a) only one and (b) both of the adjacent rigid, massless foundations with $B_f=2$ m and $d_{\mathrm{f1f2}}=8$ m resting on the surface of a homogeneous halfspace (—) and a halfspace with a stiff cylindrical inclusion (Infill D) (—) with $H=4$ m and $R=3$ m, obtained with the post processing procedure.

presumably because the center of the foundation is located besides the stiff inclusion. Especially in the high frequency range a comparably small influence of the inclusion turns out, whereas for low excitation frequencies some smaller oscillations of $|C_{zz}^{11}|$ due to interaction effects with the inclusion are visible. Furthermore a considerably decreased compliance $|C_{zz}^{21}|$ due to presence of the stiff inclusion, acting as wave barrier, is observed. In general larger $|C_{zz}^{21}|$ occur in case of $B_f=4$, as then distance of foundation edges is smaller and the mutual interaction effects are therefore stronger.

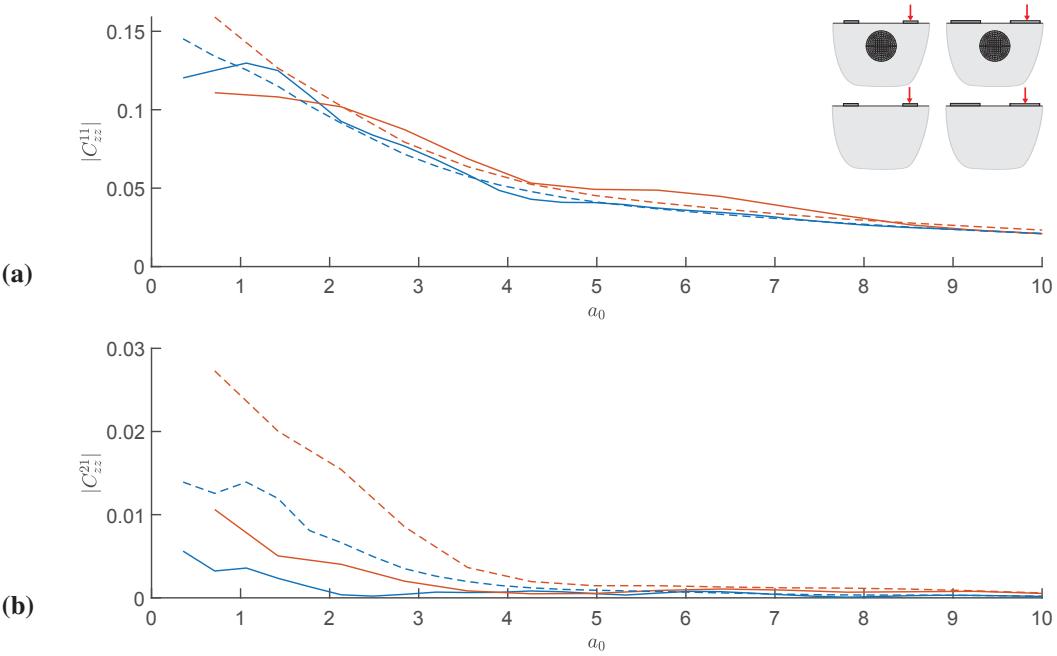

Figure 19: Absolute vertical compliance functions $|C_{zz}^{ij}(a_0)|$ for (a) first (loaded) and (b) second of two adjacent rigid, massless square foundations with $B_f=2$ m (—), $B_f=4$ m (—) and distance $d_{\mathrm{f1f2}}=8$ m on halfspace with cylindrical inclusion (Infill D) with embedment depth $H=3$ m and radius $R=2$ m (solid lines) and on a homogeneous halfspace (dashed lines).

Variation of foundation distance d_{f1f2}

The variation of the midpoint distance d_{f1f2} in Fig. 20 for a constant foundation width as well as inclusion size, location and material shows, that the cross interaction between the foundations decreases with increasing distance regardless the underlying soil. For a homogeneous halfspace, $|C_{zz}^{11}|$ of the loaded foundation is equal for all d_{f1f2}, whereas the influence of the inclusion is clearly visible for small distances of the foundations and decreases with increasing d_{f1f2}, thereby converging to the halfspace solution. In general larger $|C_{zz}^{21}|$ are observed for the homogeneous halfspace, which also decrease with increasing d_{f1f2} and a_0. Due to the rather large inclusion located closely to the halfspace surface, only very low compliance values $|C_{zz}^{21}|$ show up for larger foundations distances. For the likewise nearby foundations with $d_{\mathrm{f1f2}} = 4$ m, an increase of the compliance amplitude above the first horizontal resonance frequency of the soil layer at $a_0 = 3.14$ can be observed and attributed to the then possible propagation of surface waves, passing through the soil over the inclusion and impinging at the second foundation.

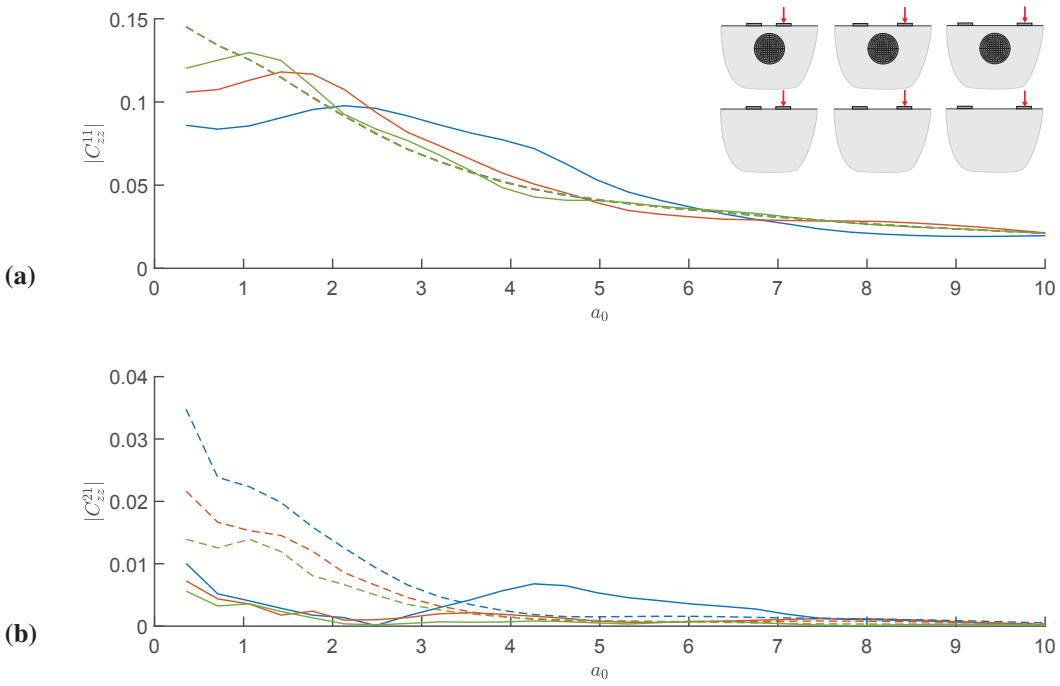

Figure 20: Absolute vertical compliance functions $|C_{zz}^{ij}(a_0)|$ for (a) first (loaded) and (b) second of two adjacent rigid, massless square foundations with $B_f = 2$ m on halfspace with cylindrical inclusion (Infill D) with embedment depth $H = 3$ m and radius $R = 2$ m (solid lines) and on a homogeneous halfspace (dashed lines) for varying distance $d_{\mathrm{f1f2}} = 4$ m (—), $d_{\mathrm{f1f2}} = 6$ m (—) and $d_{\mathrm{f1f2}} = 8$ m (—).

Variation of inclusion stiffness E_{cyl}

Finally, the effect of a varying stiffness of the inclusion is investigated. Therefore the Young's modulus E_{cyl} is adapted such that the ratio of the shear wave velocity of the infill material and the soil $c_{\mathrm{s,cyl}}/c_s$ takes values between 2 and 8, additionally to the very stiff inclusion with $c_{\mathrm{s,cyl}}/c_s = 37.6$ investigated in the previous cases.

The vertical compliance of the active foundation $|C_{zz}^{11}|$ in Fig. 21a generally differs only slightly from the results for the homogeneous halfspace. However, an increase of the smooth peak in the low frequency range and an ascending waviness of the course of the compliance is observed for raising stiffness of the inclusion. The compliance of the passive foundation $|C_{zz}^{21}|$

in Fig. 21b drastically reduces with increasing stiffness E_{cyl}. The oscillations in $|C_{zz}^{21}|$ imply, that, in dependency of the frequency and with that the corresponding wavelengths, the elastic waves interact differently with the inclusion and the wave field resulting from the direct and reflected waves at the inclusion shows amplification and attenuation effects compared to the nearly monolithically decaying of the compliance $|C_{zz}^{21}|$ in case of the homogeneous halfspace.

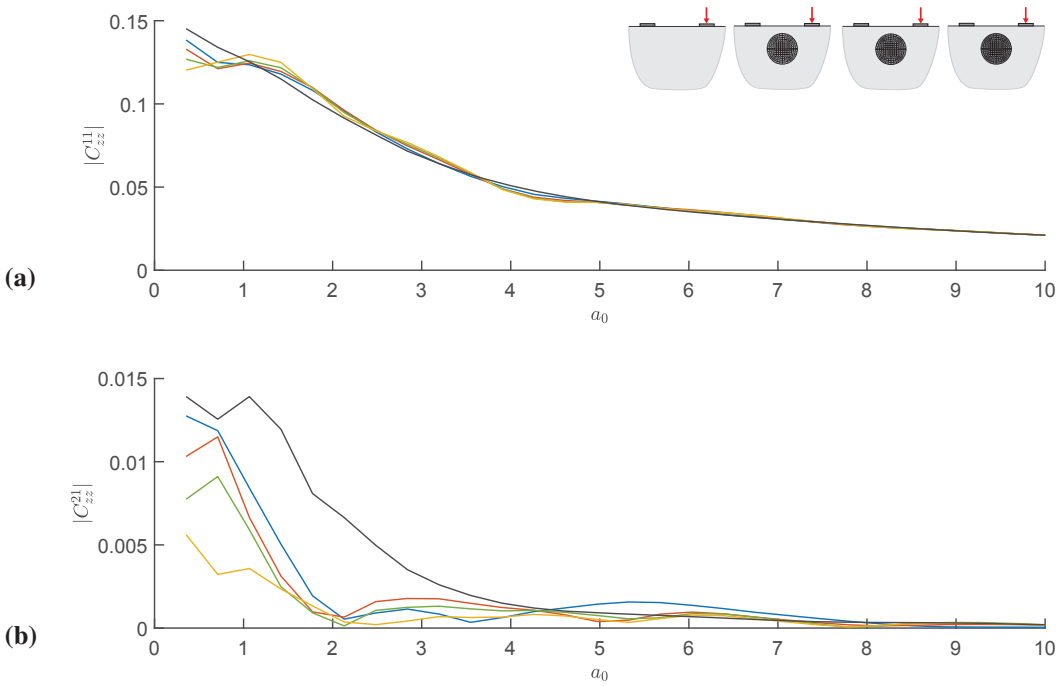

Figure 21: Absolute vertical compliance functions $|C_{zz}^{ij}(a_0)|$ for (a) first (loaded) and (b) second of two adjacent rigid, massless square foundations with $B_f = 2$ m and distance $d_{\mathrm{f1f2}} = 8$ m on halfspace with cylindrical inclusion with embedment depth $H = 3$ m and radius $R = 2$ m for varying stiffness of inclusion: Infill A $c_{\mathrm{s,cyl}} = 141.4$ ms^{-1} (—), Infill B $c_{\mathrm{s,cyl}} = 282.8$ ms^{-1} (—), Infill C $c_{\mathrm{s,cyl}} = 565.68$ ms^{-1} (—), Infill D $c_{\mathrm{s,cyl}} = 2661.45$ ms^{-1} (—) and on a homogeneous halfspace (—).

5 CONCLUSIONS

In this paper an efficient approach for the investigation of the dynamic interaction of finite, three dimensional foundations located on the surface of a soil with a buried local, length invariant structure or inhomogeneity is presented. A 2.5D ITM-FEM approach was used for the determination of the complex, dynamic stiffness matrix of the soil substructure, which is coupled to the dynamic stiffness of the foundations (modelled with conventional 3D finite elements), at the common interaction surfaces via the compatibility conditions. Frequency dependent, dimensionless compliance functions of rigid, massless surface foundations resting on a homogeneous halfspace, modelled with the presented approach by choosing the same material properties for the inclusion as for the surrounding soil, were computed and compared to literature results, showing very good agreement and thereby validating the proposed methodology.

The approach was applied to compute the dynamic response of a single or two adjacent surface foundations, taking into account the through soil coupling as well as the interaction with the inclusion inside the soil, for different system configurations. The influence of both, the embedment depth, size and stiffness of the inclusion and the width and distance of the foundations on the compliance functions at the soil foundation interface was investigated.

In general the impact of the inclusion on the response is larger, if it is located closely to the foundations and features a rather large size in comparison to the elastic wavelengths at the corresponding frequency. With increasing distance of the foundations, as well as for raising embedment depths, decreasing inclusion sizes or a reduced stiffness the compliance functions converge to the results for the case, where the foundations are resting on a homogeneous half-space. For the response at the unloaded foundation the resonance frequency of the soil layer over the inclusion showed to play a decisive role, as below this cut-off frequency a propagation of free waves through this soil layer in the transmission path between the two foundations is not possible. This effect, in combination with the behaviour of the inclusion as a wave barrier, leads to a very small reception at the passive foundation, if the excitation frequency is below this first critical frequency.

Furthermore, the displacement field resulting from the interaction of two adjacent surface foundations with a soil including a stiff cylindrical confinement, due to a dynamic excitation of either one or both, was presented. Thereby a significant reduction in displacement amplitudes at the surface was observed in a limited area along the entire length of the stiff inclusion compared to the case of a homogeneous soil, which in turn led to an increase in amplitudes in the direction perpendicular to the inclusion on both sides, in case both foundations are loaded. For a load only on one foundation, the stiff inclusion shows to act as a wave barrier, leading to significantly reduced displacement amplitudes on the opposite site of the confinement.

REFERENCES

[1] H. L. Wong, J. E. Luco, Dynamic response of rigid foundations of arbitrary shape, Earthquake Engineering & Structural Dynamics 4 (1976) 579–587.

[2] J. Dominguez, J. M. Roesset, Dynamic stiffness of rectangular foundations, Nasa Sti/recon Technical Report N 79 (1978).

[3] S. A. Savidis, T. Richter, Dynamic response of elastic plates on the surface of the half-space, International Journal for Numerical and Analytical Methods in Geomechanics 3 (1979) 245–254.

[4] M. Iguchi, J. E. Luco, Dynamic response of flexible rectangular foundations on an elastic half-space, Earthquake Engineering & Structural Dynamics 9 (1981) 239–249.

[5] H. R. Hamidzadeh-Eraghi, P. Grootenhuis, The dynamics of a rigid foundation on the surface of an elastic half-space, Earthquake Engineering & Structural Dynamics 9 (1981) 501–515.

[6] W. L. Whittaker, P. Christiano, Dynamic response of plate on elastic half-space, Journal of the Engineering Mechanics Division 108 (1982) 133–154.

[7] H. Antes, O. von Estorff, Dynamic response analysis of rigid foundations and of elastic structures by boundary element procedures, Soil Dynamics and Earthquake Engineering 8 (1989) 68–74.

[8] O. von Estorff, E. Kausel, Coupling of boundary and finite elements for soil-structure interaction problems, Earthquake Engineering & Structural Dynamics 18 (1989) 1065–1075.

[9] G. B. Warburton, J. D. Richardson, J. J. Webster, Forced vibrations of two masses on an elastic half space, Journal of Applied Mechanics 38 (1971) 148–156.

[10] T. Kobori, R. Minai, K. Kusakabe, Dynamical characteristics of soil-structure cross-interaction system, i (1973).

[11] H. L. Wong, J. E. Luco, Dynamic interaction between rigid foundations in a layered half-space, Soil Dynamics and Earthquake Engineering 5 (1986) 149–158.

[12] E. Kausel, J. M. Roesset, G. Waas, Dynamic analysis of footings on layered media, Journal of Engineering Mechanics 101 (1975).

[13] H.-T. Lin, J. M. Roesset, J. L. Tassoulas, Dynamic interaction between adjacent foundations, Earthquake Engineering & Structural Dynamics 15 (1987) 323–343.

[14] T. Triantafyllidis, B. Prange, Dynamic subsoil-coupling between rigid rectangular foundations, Soil Dynamics and Earthquake Engineering 6 (1987) 164–179.

[15] D. L. Karabalis, D. E. Beskos, Dynamic response of 3-d rigid surface foundations by time domain boundary element method, Earthquake Engineering & Structural Dynamics 12 (1984) 73–93.

[16] J. Qian, D. E. Beskos, Harmonic wave response of two 3-d rigid surface foundations, Soil Dynamics and Earthquake Engineering 15 (1996) 95–110.

[17] J. Qian, L. G. Tham, Y. K. Cheung, Dynamic analysis of rigid surface footings by boundary element method, Journal of Sound and Vibration 214 (1998) 747–759.

[18] Y. Wang, R. K. N. D. Rajapakse, A. H. Shah, Dynamic interaction between flexible strip foundations, Earthquake Engineering & Structural Dynamics 20 (1991) 441–454.

[19] D. C. Rizos, Z. Wang, Coupled bem–fem solutions for direct time domain soil–structure interaction analysis, Engineering Analysis with Boundary Elements 26 (2002) 877–888.

[20] X. Chen, C. Birk, C. Song, Transient analysis of wave propagation in layered soil by using the scaled boundary finite element method, Computers and Geotechnics 63 (2015) 1–12.

[21] B. Sbartai, Dynamic interaction of two adjacent foundations embedded in a viscoelastic soil, International Journal of Structural Stability and Dynamics 16 (2016) 1450110.

[22] Z. Han, G. Lin, J. Li, Dynamic 3d foundation–soil–foundation interaction on stratified soil, International Journal of Structural Stability and Dynamics 17 (2017) 1750032.

[23] M. Radisic, Itm-based dynamic analysis of foundations resting on a layered halfspace, Ph.D. thesis, Universität Belgrad, Belgrad, 2018.

[24] N. Chouw, R. Le, G. Schmid, Propagation of vibration in a soil layer over bedrock, Engineering Analysis with Boundary Elements 8 (1991) 125–131.

[25] N. Chouw, G. Schmid, Building isolation using the transmitting behaviour of a soil layer, in: Proceedings of the 10th world conference on signal engineering, Madrid (Spain), volume 4, pp. 2519–2524.

[26] H. Takemiya, A. Fujiwara, Wave propagation/impediment in a stratum and wave impeding block (wib) measured for ssi response reduction, Soil Dynamics and Earthquake Engineering 13 (1994) 49–61.

[27] H. Antes, O. von Estorff, Dynamic response of 2d and 3d block foundations on a halfspace with inclusions, Soil Dynamics and Earthquake Engineering 13 (1994) 305–311.

[28] A. T. Peplow, S. Finnveden, Calculation of vibration transmission over bedrock using a waveguide finite element model, International Journal for Numerical and Analytical Methods in Geomechanics 32 (2008) 701–719.

[29] G. Gao, J. Chen, X. Gu, J. Song, S. Li, N. Li, Numerical study on the active vibration isolation by wave impeding block in saturated soils under vertical loading, Soil Dynamics and Earthquake Engineering 93 (2017) 99–112.

[30] C. F. Long, On the completeness of the lamè potentials, Acta Mechanica 3 (1967) 371–375.

[31] G. Müller, Ein Verfahren zur Erfassung der Fundament-Boden Wechselwirkung unter Einwirkung periodischer Lasten, Dissertation, Technische Universität München, München, 1989.

[32] A. Sommerfeld, Partial differential equations in physics, volume 1 of */Pure and applied mathematics*, Acad. Pr, New York, 1964.

[33] J. Freisinger, M. Hackenberg, G. Müller, A coupled integral transform method - finite element

method approach to model the soil structure interaction of finite (3d) and length invariant (2.5d) systems, Journal of Sound and Vibration 482 (2020) 115443.

[34] M. Hackenberg, M. Dengler, G. Müller, Implementation of the finite element method in the fourier-transformed domain and coupling with analytical solutions, in: Cunha A., Caetano E., Ribeiro P., Müller G (Ed.), Eurodyn.

[35] G. Frühe, Überlagerung von Grundlösungen in der Elastodynamik zur Behandlung der dynamischen Tunnel-Boden-Bauwerk-Interaktion, Dissertation, Technische Universität München, München, 2010.

[36] M. Hackenberg, A Coupled Integral Transform Method - Finite Element Method Approach to Model the Soil-Structure-Interaction, Dissertation, Technische Universität München, München, 2016.

[37] F. Rojas, J. C. Anderson, L. M. Massone, A nonlinear quadrilateral layered membrane element with drilling degrees of freedom for the modeling of reinforced concrete walls, Engineering Structures 124 (2016) 521–538.

[38] R. Hirschauer, Kopplung von finiten Elementen mit Rand-Elementen zur Berechnung der dynamischen Baugrund-Bauwerk-Interaktion: Zugl.: Berlin, Techn. Univ., Diss., 2001, volume 31 of *Veröffentlichungen des Grundbauinstitutes der Technischen Universität Berlin*, Univ.-Bibliothek der Techn. Univ. Abt. Publ. Sekr. FRA-B, Berlin, 2001.

[39] R. Shahi, A. Noorzad, Dynamic response of rigid foundations of arbitrary shape using half-space green's function, International Journal of Geomechanics 11 (2011) 391–398.

[40] D. L. Karabalis, M. Mohammadi, 3-d dynamic foundation-soil-foundation interaction on layered soil, Soil Dynamics and Earthquake Engineering 17 (1998) 139–152.

[41] T. Kobori, R. Minai, T. Suzuki, The dynamical ground compliance of a rectangular foundation on a viscoelastic stratum (1971).